European Journal of Medicinal Chemistry 277 (2024) 116755

Contents lists available at ScienceDirect

European Journal of Medicinal Chemistry

journal homepage: www.elsevier.com/locate/ejmech

Research paper

Synthesis and biological evaluation of novel 3,6- amide and thioamide substituted- 2,3,4,9-tetrahydro-1H-carbazoles for anti-cancer activity

Alicja Trocka [a,1], Anoop Kallingal [b,1], Natalia Maciejewska [b], Magdalena Narajczyk [c], Anna Hromova [a], Sławomir Makowiec [a,*]

[a] Department of Organic Chemistry, Faculty of Chemistry, Gdansk University of Technology, Narutowicza 11/12, 80-233, Gdansk, Poland
[b] Department of Pharmaceutical Technology and Biochemistry, Faculty of Chemistry, Gdansk University of Technology, Narutowicza 11/12, 80-233, Gdansk, Poland
[c] Bioimaging Laboratory, Faculty of Biology, University of Gdansk, Wita Stwosza 59, 80-308, Gdansk, Poland

ARTICLE INFO

Keywords:
Cancer
Carbazole
Tetrahydrocarbazole
Thioamide
DNA damage
CAM assay

ABSTRACT

Herein, we report the synthesis of new compounds with demonstrated anticancer properties based on the 2,3,4,9-tetrahydro-1H-carbazole scaffold. The Fischer indolization method was used to close the heterocyclic motif. The synthesis method's scope and limitations were thoroughly assessed through a series of experiments. Biological assays revealed that two thioamide compounds exhibited significant anticancer activity against MCF-7, HTC116, and A596 cell lines. Comprehensive *in vitro* profiling included evaluation of cell cytotoxicity, morphological alterations, colony formation and cell adhesion in 3D cultures, cell cycle analysis, DNA damage induction, impact on mitochondria, and apoptosis. *Ex ovo* studies further demonstrated these compounds' potential to inhibit angiogenic processes. Our results indicate that the newly developed compounds activate processes leading to DNA damage and disruption of mitochondrial function.

1. Introduction

Derivatives of 2,3,4,9-tetrahydro-1H-carbazole (THCZ), otherwise referred to as carbazole derivatives, are a significant class of organic compounds possessing a plethora of intriguing pharmacological properties [1–3]. Several synthetic and natural compounds that encompass this particular structural scaffold have been documented in scientific literature, demonstrating diverse biological activities. One of the noteworthy examples pertains to the pharmacological agent that falls under the category of selective agonists of serotonin 5-HT1B/1D receptors. One such compound is utilized in the management of migraine symptoms and is commercially available as Frovatriptan (**1**) [4]. Another example is Ondansetron (**2**), a tetrahydrocarbazole derivative with antiemetic properties, used for the management of chemotherapy- and radiotherapy-induced nausea [5]. Apart from the pharmaceuticals that have been approved and contain the tetrahydrocarbazole core, there exist a myriad of experimental substances containing this structural motif. These include compounds that bear potential antimicrobial attributes, for instance, the chemical species - referred to as GSK983 (IC_{50} = 0.005 μM) (**3**) which exhibits antiviral activity. Extensive *in vitro* examinations have shown that this chemical compound exerts a blocking influence on the replication of several viruses, including Ad-5 adenovirus, SV-40 poliomyelitis virus, Epstein-Barr virus (EBV), and human papillomavirus (HPV) [6]. Moreover, aside from demonstrating antiviral efficacy, tetrahydrocarbazole derivatives exhibit potential bactericidal effect (IC_{50} = 115 μM) (**4**) [7]. The hybrid molecule of tetrahydrocarbazole, incorporating a 2,4-diaminopyrimidine scaffold (**5**), exhibited significant activity against both *S. aureus* Newman (MIC = 0.39–0.78 μg/mL) and *Escherichia coli* AB1157 (MIC = 0.39–0.78 μg/mL), as well as to multi-drug-resistant *S. aureus* pathogens. The observed efficacy of this compound is similar to that of the antibacterial agent Wacomycin [8]. Furthermore, the scientific evidence has demonstrated that molecules possessing a THCZ scaffold exhibit a wide range of antifungal properties [9]. In addition to its proven antimicrobial activity, the structural motif is also implicated in the treatment of autoimmune disorders. BMS-986142 (IC_{50} = 0.090 μM) (**6**), an anti-inflammatory agent targeted towards the treatment of rheumatoid arthritis, is currently undergoing clinical trials to evaluate its efficacy and safety [10]. THCZ moiety is an essential constituent of the molecular architecture of Flutriciclamide (18F-GE180) (**7**), a neurodiagnostic

* Corresponding author.
E-mail address: mak@pg.edu.pl (S. Makowiec).
[1] These authors contributed equally.

https://doi.org/10.1016/j.ejmech.2024.116755
Received 13 June 2024; Received in revised form 5 August 2024; Accepted 6 August 2024
Available online 11 August 2024

compound used for the detection and surveillance of brain inflammation, which is crucial in managing neurological disorders [11]. Moreover, various THCZ derivatives, including sorazolones (**8**), kopsihainanins (IC_{50} = 38.5 μM) (**9**) and leucomidins (IC_{50} > 100 μM) (**10**) have also been identified and discussed [12–14]. Chemical structures of tetrahydrocarbazole derivatives used in approved therapies and experimental studies are included in this paper (Scheme 1).

In the extant literature, there exists a plethora of investigations dedicated to scrutinizing the anticancer properties of carbazoles (Scheme 2). Pei and co-workers demonstrated that the tetrahydrocarbazole derivative of 1-(4-chloro-3-(fluoromethyl)phenyl)urea (RAW 264.7 EC_{50} = 17.18 μM, BMDM EC_{50} = 18.87 μM) (**11**), containing the 1-methyl-1H-pyrazole moiety, could have a significant potential as a TAM modulator in the context of switching the TAM polarization state in cancer [15]. Other research groups focused on the biological efficacy of tetrahydrocarbazole hybrids in conjunction with dithioate derivatives was scrutinized. Emphasis was placed on the structure comprising of the 1-(4-chlorophenyl)piperazine moiety (MCF-7 IC_{50} = 7.24 μM, HCT116 IC_{50} = 8.23 μM) (**12**), which exhibited remarkably efficient cytotoxic potential as determined by *in vitro* screening tests conducted on the MCF-7 cell line. It is noteworthy that the cytotoxic activity of this structure surpassed that of doxorubicin, the reference pharmaceutical employed in the studies [16]. Additionally, the synthesized 15-methylene-eburnamine molecule (MDA-MB-231 IC_{50} = 14.1 μM, LNCaP IC_{50} = 9.5 μM, RPMI-8226 IC_{50} = 12.2 μM, U266 IC_{50} = 4.3 μM, KMS-12BM IC_{50} = 4.0 μM) (**13**) derived from the natural eburnamine compound extracted from *Catharanthus roseus*, was found to exhibit antiproliferative activity in HL-60 cells and cytotoxicity against different cancer cells [17]. It was investigated also the Mannich bases of 9-alkyl-1,2,3,4-tetrahydrocarbazol-1-ones. *In vitro* assays revealed that the structure incorporating a diethylaminomethyl moiety (A549 IC_{50} = 110.41 μM, SGC IC_{50} = 24.37 μM, K562 IC_{50} = 17.30 μM, HCT116 IC_{50} = 2.96 μM, KB-R IC_{50} = 117.58 μM) (**14**) exhibited noteworthy potential as an agent against the HCT116 cell line. The observed cytotoxic potency was determined to be 35-fold higher than that of taxol [18]. Our research group have recently conducted experiments on 1,2,3,6-tetrasubstituted aminocarbazoles and their impact on various human cancer cell lines *in vitro*. As a consequence of these research investigations, two chemical structures were discerned to possess noteworthy inhibitory capability on the proliferation of HCT116 and U2OS cells, compared by 5-fluorouracil, which served as the experimental control [19].

THCZ derivatives can be prepared using a broad scope of methods [20–27]. In the context of our research, with the goal of closing the tricyclic tetrahydrocarbazole system, we opted to employ the Fischer indolization methodology [28]. By this approach, an assortment of commercially procurable substrates may be utilized, including a broad spectrum of ketones in combination with diverse phenylhydrazine derivatives. To increase the chances of success during the initial screening studies, we also decided to apply thionation of the prepared amides, assuming that there is a high probability of finding a molecule with the desired biologically activity among the thioamide derivatives due to their specific chemical properties [29].

Throughout the preceding two decades, numerous tetrahydrocarbazole derivatives exhibiting anticancer potential have been discerned. However, the escalating occurrence of chemoresistance across various cancers underscores the significance of continued research endeavors and exploration for new compounds. In the present study, we developed the synthesis of a novel set of 3,6-substituted 2,3,4,9-tetrahydro-1H-carbazole and their thioamide derivatives, along with an analysis of their antiproliferative activity on diverse cancer cell lines.

2. Results and discusion

2.1. Chemistry

An important problem in the context of synthesizing potential anticancer compounds is the formation of the 2,3,4,9-tetrahydro-1H-carbazole scaffold. There are many methods in the literature for closing this structural motif, as mentioned in the introduction. For this research, the chosen reaction was the Fischer indolization method, which is a universal reaction with a wide application in both the industry and the scientific community. The planned synthesis pathways are shown above (Scheme 3). A wide range of hydrazines and ketones are commercially available, which allows for easy modification of the designed compounds. In the synthesis of FI, phenylhydrazine hydrochlorides (**15a-**

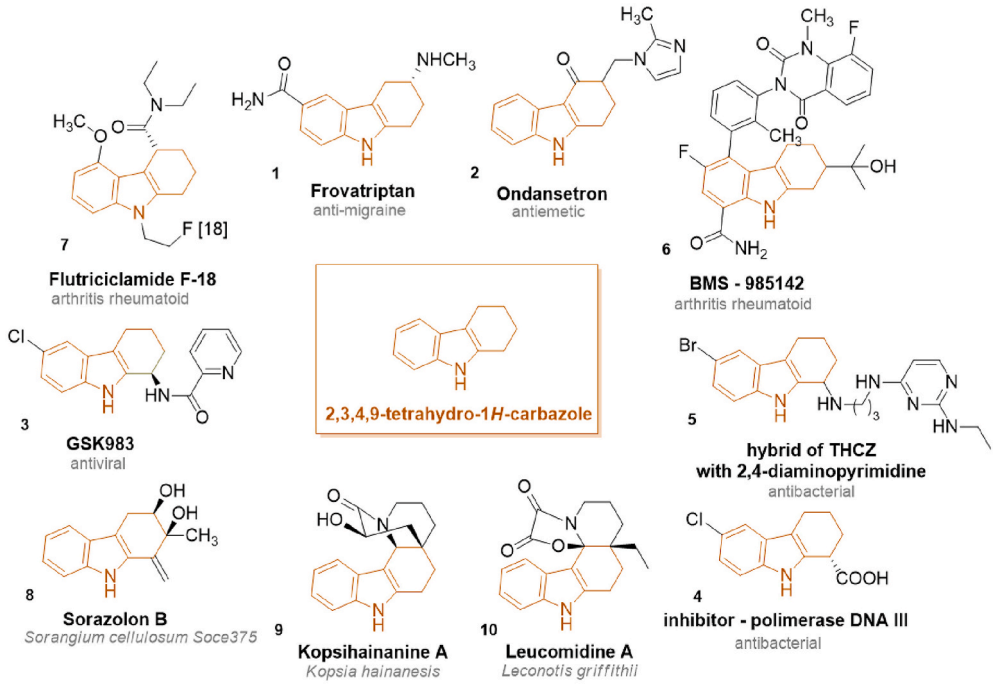

Scheme 1. Chemical structures of tetrahydrocarbazole derivatives used in approved therapies and experimental studies.

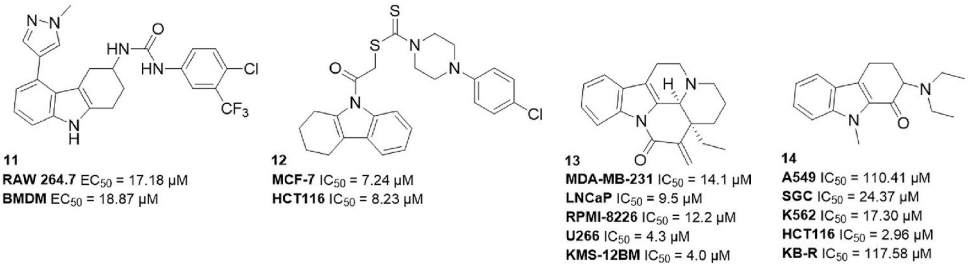

Scheme 2. Chemical structures of tetrahydrocarbazole derivatives, which have been used as potential anticancer substances.

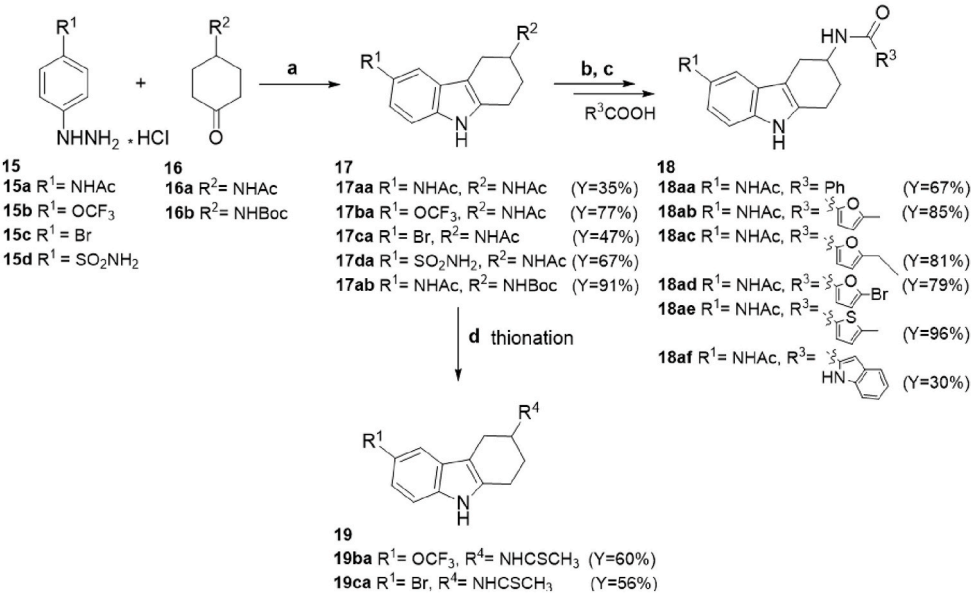

Scheme 3. Reagents and conditions used for the preparation of compounds based on 3,6-Substituted 2,3,4,9-Tetrahydro-1H-carbazoles scaffold: (a) EtOH, 79 °C, 24 h; (b) TFA, DCM, rt, 1h; (c) DMF, TBTU, TEA, rt, 24 h; (d) P_2S_5, dry dioxane, RT, 24 h. The reaction yields are given in brackets.

15d) and ketones (**16a-16b**) were used as starting materials. Two types of 4-substituted cyclohexanones were utilized. N-(4-oxocyclohexyl) acetamide (**16a**), which has a difficult-to-remove N-acetamide moiety, was employed to prepare intermediates that were then subjected to the thionation reaction. On the other hand, *tert*-butyl (4- oxocyclo-hexyl) carbamate (**16b**) was used to ensure easy deprotection of the protecting group (-Boc) and thus for the preparation of free 2,3,4,9-tetrahydro-1H-carbazol-3-amine for subsequent derivatization from selected acyl groups. The first step (**a**) was optimally performed under standard conditions, where 1 equivalent of ketone was treated with 1 equivalent of hydrazine hydrochloride salt in boiling ethanol for 24 h. The yields and purity of the obtained compounds (**17aa-17ab**) were satisfactory in most reactions, ranging from 35 % to 91 %. However, synthetic problems were encountered when combining trifluoromethoxy (**15b**) and 4-bromo (**15c**) phenylhydrazines with a ketone (-Boc) (**16b**). It was not possible to obtain the desired products due to the significant decomposition of the products and the inability to purify them using flash chromatography. Attempts were made to optimize the method by changing factors such as solvent, temperature, and conducting the reaction in the dark, but all of these attempts were unsuccessful. It is worth emphasizing that in the case of free basic hydrazines, it is necessary to introduce gaseous HCl into the reaction mixture to achieve a positive result. Due to problems with the lability of the (-Boc) protecting group, only one compound could be prepared, namely *tert*-butyl (6-acetamido-2,3,4,9-tetrahydro-1H-carbazol-3-yl)carbamate (**17 ab**).

Tert-butyl (6-methyl-2,3,4,9-tetrahydro-1H-carbazol-3-yl)carbamate (**17 ab**) was deprotected under standard conditions using trifluoroacetic acid (TFA) in dichloromethane (DCM) (**b**). The obtained amine trifluoroacetate was used as a substrate for the next reaction step. The amine was coupled with an aromatic carboxylic acid (mostly furoyl) using TBTU as an activating agent in N,N-dimethylformamide (DMF) (**c**). N-(6-substituted-2,3,4,9-tetrahydro-1H-carbazol-3-yl)acetamides (**17aa-17da**) were subjected to thionation (**d**) process. Thionation was successfully carried out in the case of N-(6-trifluoromethoxy-2,3,4,9-tetrahydro-1H-carbazol-3-yl)acetamide (**17ba**) and N-(6-bromo-2,3,4,9-tetrahydro-lH-carbazol-3-yl)acetamide (**17ca**) using P_2S_5 as sulphurating agent. However, in the case of N-(6-acetamido-2,3,4,9-tetrahydro-1H-carbazol-3-yl)acetamide (**17aa**), we encountered selectivity issues during sulfurization, as a difficult to separate mixture of mono- and dithionated product was obtained. Furthermore, in the case of thionation of molecule (**17da**), the resulting compound was unstable and several side products were observed on the TLC plate.

2.1.1. Biological evaluation

2.1.1.1. Cell cytotoxic evaluation. The cytotoxicity of 12 synthesized compounds was evaluated on breast adenocarcinoma cells (MCF-7), non-small cell lung carcinoma cells (A549) and colon carcinoma cells (HCT116) using the MTT assay. Out of the 12 compounds, two compounds, (**19ba**) and (**19ca**), demonstrated activity against the three cell lines. The half-maximal inhibitory (IC_{50}) values for (**19ba**) were determined to be 30.955 ± 1.904 μM, 25.674 ± 0.291 μM, and 23.579 ± 1.648 μM for MCF-7, A549, and HCT116 cell lines respectively, and the IC_{50} values for (**19ca**) were 3.805 ± 1.32 μM, 4.544 ± 1.16 μM and

40.041 ± 4.83 μM for MCF-7, A549, and HCT116 cell lines respectively (Table 1 & Fig. 1). It is worth noting that different cancer cell lines may respond differently to the same compound, and that these results may not necessarily be directly comparable to other cell lines or *ex-ovo* studies. The molecular biological significance of these results is that it demonstrates that the compounds (**19ba**) and (**19ca**) may have the ability to inhibit the proliferation of cancer cells. The cytotoxicity of these compound is likely due to their ability to interfere with key cellular processes such as cell division, DNA replication, and apoptosis. Given that the IC_{50} values obtained in the two lines of cells exceeded 50 μM, it was unviable to further calculate the Selectivity Index. However, based on the observed results, the newly synthesized compounds, (**19ba**) and (**19ca**), demonstrate improved selective cytotoxicity in cancer cells relative to normal cells. Thus, the increased selectivity further highlights the potential use of the two compounds as effective therapeutic agents, targeting cancer tissues. The cytotoxic activity of these two compounds was further confirmed by examining morphological changes in A549, MCF-7, and HCT116 cell lines through visualization by fluorescent microscopy as shown **in** Fig. 2-AC and described in the **Supplementary Information**.

2.1.1.2. Inhibitory effects of novel compounds on colony formation and cellular adhesion in 3D cultures. In cancer research, the ability of tumor cells to form colonies is a critical metric, reflecting tumor malignancy and implications for recurrence and therapy resistance. Our study aimed to assess the long-term survival potential of tumor cells following treatment by evaluating their clonogenic capacity [30,31].

Experiments using MCF-7, HCT116, and A549 cell lines showed a significant reduction in clonogenic capacity when treated with specific compounds compared to untreated counterparts, as depicted in Fig. 2E. This reduction indicates a substantial decrease in the number of surviving cells capable of proliferating highlighting the effectiveness of the treatment. Notably, compound (**19ca**) showed heightened sensitivity in MCF-7 and A549 cell lines, whereas compound (**19ba**) was more effective against the HCT116 cell line. This differential sensitivity was quantitatively illustrated through a dose-dependent decrease in colony formation as shown in Fig. 2D. These observations suggest that the two compounds may interfere with cellular mechanisms in a cell-type-specific manner, pivotal for developing targeted therapeutic strategies.

Additionally, cellular adhesion experiments conducted over a 48-h period using the IC_{50} concentrations of the compounds assessed their impact on cellular adhesion within a three-dimensional (3D) culture environment (Fig. 3). These studies demonstrated that the compounds significantly influenced cellular adhesion processes. Compound (**19ca**) significantly prevented the formation of cancer cell aggregates in both A549 and MCF-7 cell lines (Fig. 3A–B), while compound (**19ba**) displayed moderate inhibition of aggregate formation in HCT116 and A549 cells (Fig. 3B–C), suggesting variable efficacy across different cellular environments. These findings highlight the potential of compounds (**19ca**) and (**19ba**) as therapeutic agents in disrupting tumor cell aggregation, a critical factor in cancer progression. Further studies are required to elucidate the mechanisms by which these compounds inhibit adhesion, whether they directly interact with specific adhesion molecules or influence the extracellular matrix. Comprehensive *in vitro* and *in vivo* studies are needed to better understand the therapeutic potential and safety profile of these compounds in cancer treatment.

2.1.1.3. Impact of compounds on cell cycle progression in cancer cell lines. This study evaluates the differential effects of the compounds (**19ca**), (**19ba**), and the reference chemotherapeutic agent Mitoxantrone (MTX)

Table 1
IC_{50} values of all tested compounds.

cell lines				
compound	MCF-7	A549	HCT116	MRC5
	IC_{50} (μM)			
17aa	>50	>50	>50	>50
17da	>50	>50	>50	>50
17ab	>50	>50	>50	>50
18aa	>50	>50	>50	>50
18ab	>50	>50	>50	>50
18ac	>50	>50	>50	>50
18ad	>50	>50	>50	>50
18ae	>50	>50	>50	>50
18af	>50	>50	>50	>50
19ba 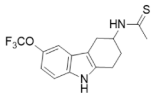	30.955 ± 1.904	25.674 ± 0.291	23.579 ± 1.648	>50
19ca 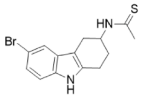	3.805 ± 1.32	4.544 ± 1.16	40.041 ± 4.83	>50
MTX	0.018 ± 0.003	0.164 ± 0.054	0.127 ± 0.015	0.517 ± 0.053
Cisplatin	30.56 ± 2.54	28.54 ± 1.64	22.61 ± 2.03	19.48 ± 2.12

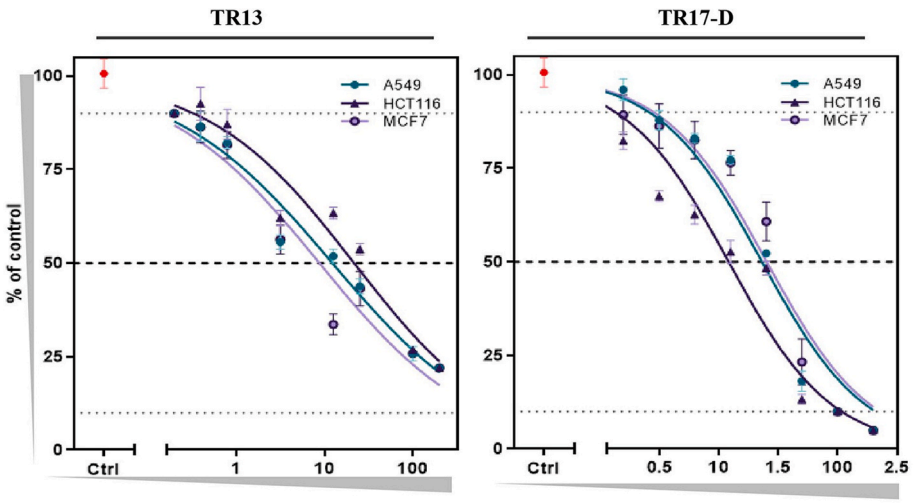

Fig. 1. The IC_{50} comparison of compounds (**A**) (**19ba**) and (**B**) (**19ca**) on HCT116, MCF-7 and A549 cells.

on cell cycle modulation within A549, HCT116, and MCF-7 cancer cell lines over periods of 24 and 48 h. In the A549 cell line, initial findings from the 24-h exposure period demonstrated a normal cell cycle distribution within the untreated control group: 37.40 ± 2.40 % of cells in G1 phase, 39.41 ± 2.54 % in S phase, and 23.45 ± 1.62 % in G2 phase. In comparison, treatment with compound (**19ca**) resulted in a notable decrease in cells in G1 (31.6 ± 3.07 %) and S phases (27.15 ± 1.16 %), with a significant reduction in the progression to G2 phase (14.3 ± 2.43 %). These results suggest potential DNA damage or replication stress-induced delays. In contrast, cells treated with compound (**19ba**) displayed a significant reduction in S phase occupancy (15.45 ± 3.76 %), indicative of S-phase arrest. MTX treatment resulted in an increase in G1 phase (34.65 ± 2.192 %) and a concomitant decrease in G2 phase (20.2 ± 1.55 %), consistent with its known mechanism of inducing DNA damage. After 48 h of incubation, the untreated control group exhibited increases in G1 (53.5 ± 4.01 %) and G2 phases (38.15 ± 1.80 %), with a decrease in S phase (17.825 ± 3.70 %). Conversely, cells treated with (**19ca**) showed a lower G1 phase (46.15 ± 0.77 %) but an elevated S phase (30.9 ± 2.82 %). Treatment with (**19ba**) resulted in a high retention of cells in G1 (53.35 ± 0.91 %) and an increased G2 phase (46.75 ± 1.75 %), suggesting possible G2/M checkpoint activation or mitotic arrest. Meanwhile, MTX treatment maintained high G1 phase retention (48.61 ± 4.1 %) and decreased G2 phase presence (29.80 ± 0.99 %), aligning with its role in DNA damage induction (Fig. 4A).

The compounds, after a 24-h treatment with MCF-7 cells, revealed the following cell cycle distribution: treatment with (**19ca**) modestly reduced the G1 phase (33.7 ± 3.25 %) and S phase (25.65 ± 2.61 %), while increasing the G2 phase (25.95 ± 0.63 %). Methotrexate (MTX) significantly altered cell distribution, increasing G1 phase presence (44.4 ± 1.41 %) and G2 phase (33.2 ± 0.84 %), but reducing the S phase (17.9 ± 0.56 %), consistent with G1 arrest. After a 48-h incubation, treatment with (**19ca**) promoted S phase entry, suggestive of a delay in the G2/M transition, while MTX exhibited a less pronounced cell cycle arrest compared to the 24-h interval (Fig. 4B).

In HCT116 cells, the 24-h incubation revealed that treatment with (**19ba**) led to a significant decrease in the G1 (16.95 ± 0.07 %) and G2 phases (17.95 ± 2.19 %), indicating an accelerated transition from G1 to S phase. MTX increased the G2 phase presence to 26.30 ± 1.27 %, suggestive of a G2/M phase arrest. After 48 h, (**19ba**) increased G1 phase presence to 31.15 ± 2.61 % and reduced the S phase (18.90 ± 1.98 %), indicating a block at the G1/S transition. MTX demonstrated consistent cell cycle disruption across phases (Fig. 4C).

*2.1.1.4. Induction of DNA damage by experimental compounds (**19ca**) and (**19ba**) in cancer cell lines.* Flow cytometric analysis of DNA damage response using γH2AX as a marker provides crucial insights into the efficacy of anticancer compounds in inducing DNA breaks, a key mechanism exploited in cancer treatment. In this study, DNA damage induced by two experimental compounds, (**19ca**) and (**19ba**), as well as the established chemotherapeutic agent Mitoxantrone (MTX), was quantitatively assessed in MCF-7, HCT116, and A549 cell lines over 24 and 48 h. For MCF-7 cells, the control group showed minimal γH2AX positivity (5.89 ± 0.76 % at 24 h and 7.58 ± 1.23 % at 48 h), reflecting low baseline DNA damage. Upon treatment with (**19ca**), the percentage of γH2AX positive cells more than doubled by 48 h (16.78 ± 1.95 %), indicating significant DNA damage. MTX showed even more pronounced effects, with γH2AX positive cells rising to 23.01 ± 3.69 % at 48 h, highlighting its robust DNA damaging capacity (Fig. 5B). HCT116 cells exhibited a similar control γH2AX positivity (5.81 ± 2.31 % at 24 h) which slightly increased in controls at 48 h (6.24 ± 1.94 %). However, DNA damage markedly increased with both (**19ba**) and MTX treatments. After 48 h, MTX treatment resulted in the highest DNA damage (32.47 ± 4.83 %), whereas (**19ba**) also showed significant induction (14.63 ± 3.82 %). This suggests that MTX and (**19ba**) are potent inducers of DNA damage in HCT116 cells (Fig. 5C). In A549 cells, the γH2AX positivity in control were slightly similar (5.18 ± 0.64 % at 24 h and 4.90 ± 0.50 % at 48 h). Treatment with MTX led to a moderate increase in DNA damage (14.22 ± 1.86 % at 48 h). Both experimental compounds (**19ba**) and (**19ca**) showed significant increases in DNA damage, particularly over 48 h, with (**19ca**) reaching 11.98 ± 1.87 % positivity (Fig. 5A). Additionally, imumunofluorescence analysis provided qualitative insights into the effects of compounds (**19ca**) and (**19ba**) on A549, HCT116, and MCF-7 cells (Fig. 5D). The results from both the quantitative and qualitative analyses suggest that the experimental compounds, especially (**19ca**) in MCF-7 and A549 cells, and (**19ba**) in HCT116 cells, are potent inducers of DNA damage, highlighting their potential as anticancer agents. This study highlights the therapeutic potential of these novel compounds in activating DNA damage pathways, which could lead to the development of more effective and targeted cancer therapies, especially in cases where conventional treatments may be insufficient.

2.1.1.5. Impact of compound treatments on mitochondrial dynamics and membrane potential. To thoroughly understand the effects of compounds (19ba) and (19ca) on mitochondrial health and function in cancer cells, a series of comparative analyses and advanced microscopy studies were conducted. In a comparative analysis across the MCF-7, HCT116, and A549 cell lines, we observed differential responses to the treatments with compounds (**19ba**) and (**19ca**) over a 24-h period (Fig. 6). Specifically, the control (DMSO-treated) cells maintained a higher JC1

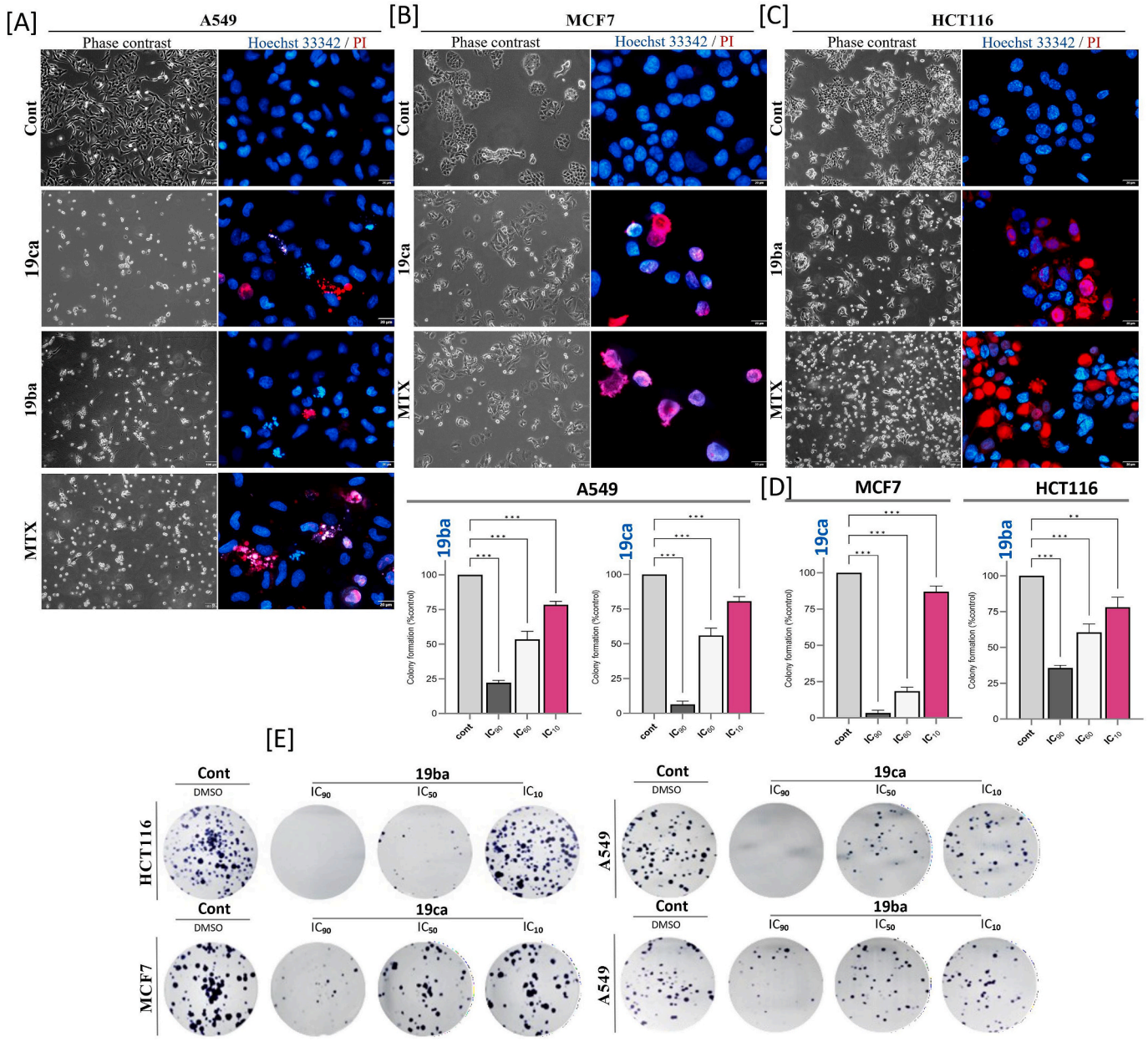

Fig. 2. Representative photomicrographs showing culture characteristics and nuclear morphology alterations in (**A**) A549, (**B**) MCF-7, and (**C**) HCT116 cell lines. (**D**) Quantification of the colony formation assay. (**E**) Representative images from the colony formation assay. Data are expressed as mean ± SEM. Significance levels are indicated as ** ($p \leq 0.01$), and *** ($p \leq 0.001$).

ratio, indicative of stable mitochondrial function. In contrast, both compounds induced a significant reduction in ΔΨm, as evidenced by the decrease in the JC1 ratio across all cell lines. The extent of this reduction varied, with compound (**19ca**) generally showing a more pronounced effect than (**19ba**). In A549 cells, the initial JC1 ratio in DMSO-treated cells was the highest at 17.72 ± 3.94, reflecting robust mitochondrial health. Treatment with compound (**19ba**) slightly reduced this ratio to 16.91 ± 0.31, suggesting a marginal impact, whereas (**19ca**) treatment halved the JC1 ratio to 8.728 ± 0.41, indicating substantial mitochondrial depolarization (Fig. 6A–B). Similarly, in MCF-7 cells, the JC1 ratio decreased from 13.4 ± 0.53 in control cells to 7.91 ± 1.22 under (**19ca**) treatment and further to 4.54 ± 0.33 with FCCP, a known mitochondrial disruptor (Fig. 6C–D). The results for HCT116 cells also reflected comparable trends with substantial decreases upon treatment with both tested compounds and FCCP (Fig. 6E–F). Additionally, mitochondrial morphology underwent significant alterations after exposure to compounds (**19ba**) and (**19ca**). Confocal microscopy revealed the formation of shortened, spherical, or circular mitochondria, indicative of enhanced mitochondrial fission (Fig. 6G & Supplementary Fig. S15). These findings underscore the sensitivity of mitochondrial function to compound-induced stress across different cancer cell types.

To elucidate the effects of mitochondrial disruption by the compounds (**19ca**) and (**19ba**), confocal microscopic analysis was employed to examine cytochrome *c* localization and behavior (Fig. 7A–C). Upon exposure to the compounds, there was a notable translocation of cytochrome *c* from the mitochondria into the cytoplasm. This migration is significant because cytochrome *c*, once in the cytoplasm, can trigger the activation of caspases that lead to apoptosis. Furthermore, released cytochrome *c* serves as a danger-associated molecular pattern (DAMP). When present outside the mitochondria, particularly in the extracellular space, it can signal immune responses and inflammation, often observed in pathological states characterized by significant cellular and

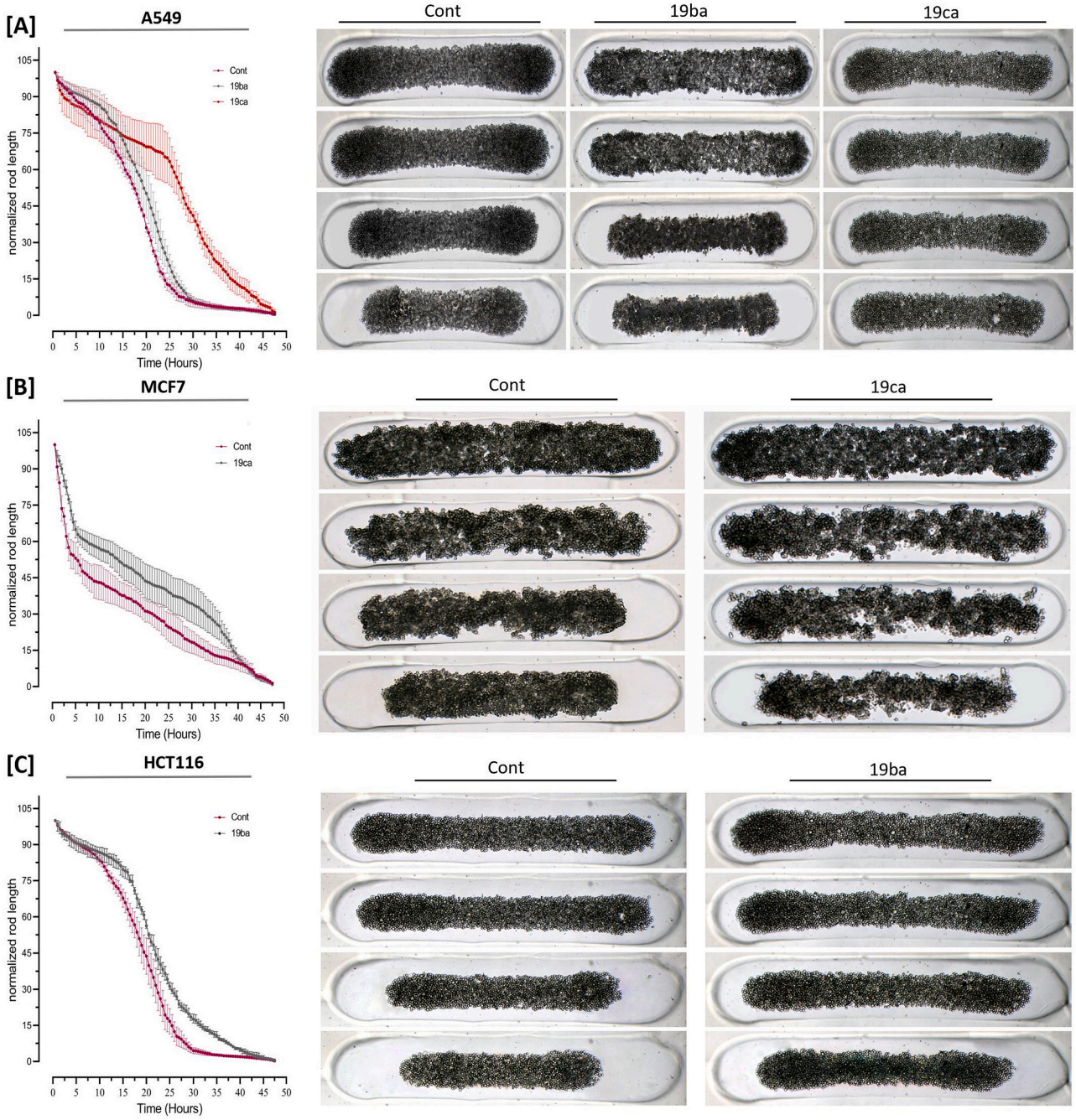

Fig. 3. Representative photomicrographs showing cell adhesion over time intervals up to 48 h via phase contrast microscopy. The lengths of individual rods were measured and normalized values are presented in corresponding graphs for (**A**) A549, (**B**) MCF-7, and (**C**) HCT116 cell lines. Data are expressed as mean ± SEM, with 15 observations per cohort. Statistical significance was noted where $p < 0.05$.

mitochondrial damage [32].

Transmission electron microscopy (TEM) analysis of compounds (**19ba**) and (**19ca**) on cancer cell lines such as A549, HCT116, and MCF-7 revealed critical morphological changes in mitochondria. These changes include significant alterations in mitochondrial size, shape, and internal organization, indicative of compromised mitochondrial integrity and function. The detailed TEM examinations suggest that the compounds induce mitochondrial swelling and a disruption of the normal distribution and organization of mtDNA nucleoids within the cells (Fig. 7D–F). This is evidenced by the presence of large, bloated mitochondria with electron-lucent regions, lacking well-developed cristae, crucial for cellular energy production. Such disruptions in mitochondrial morphology likely contribute to the induction of cell death pathways, reducing the metabolic activity within the cancer cells and ultimately leading to their death. These observed mitochondrial changes signify lasting alterations that could be fundamental to the therapeutic efficacy of these compounds.

*2.1.1.6. Induction of apoptosis by (**19ba**) and (**19ca**).* Apoptotic evaluation was performed using Annexin-V and 7-AAD staining, followed by flow cytometric analysis, to explore the capability of the compounds under study to induce apoptosis in cell cultures. The findings demonstrated that all compounds tested showed a time-dependent ability to induce apoptosis. In A549 cell line, apoptotic cells increased substantially from 24 to 48 h. The control showed a moderate increase from

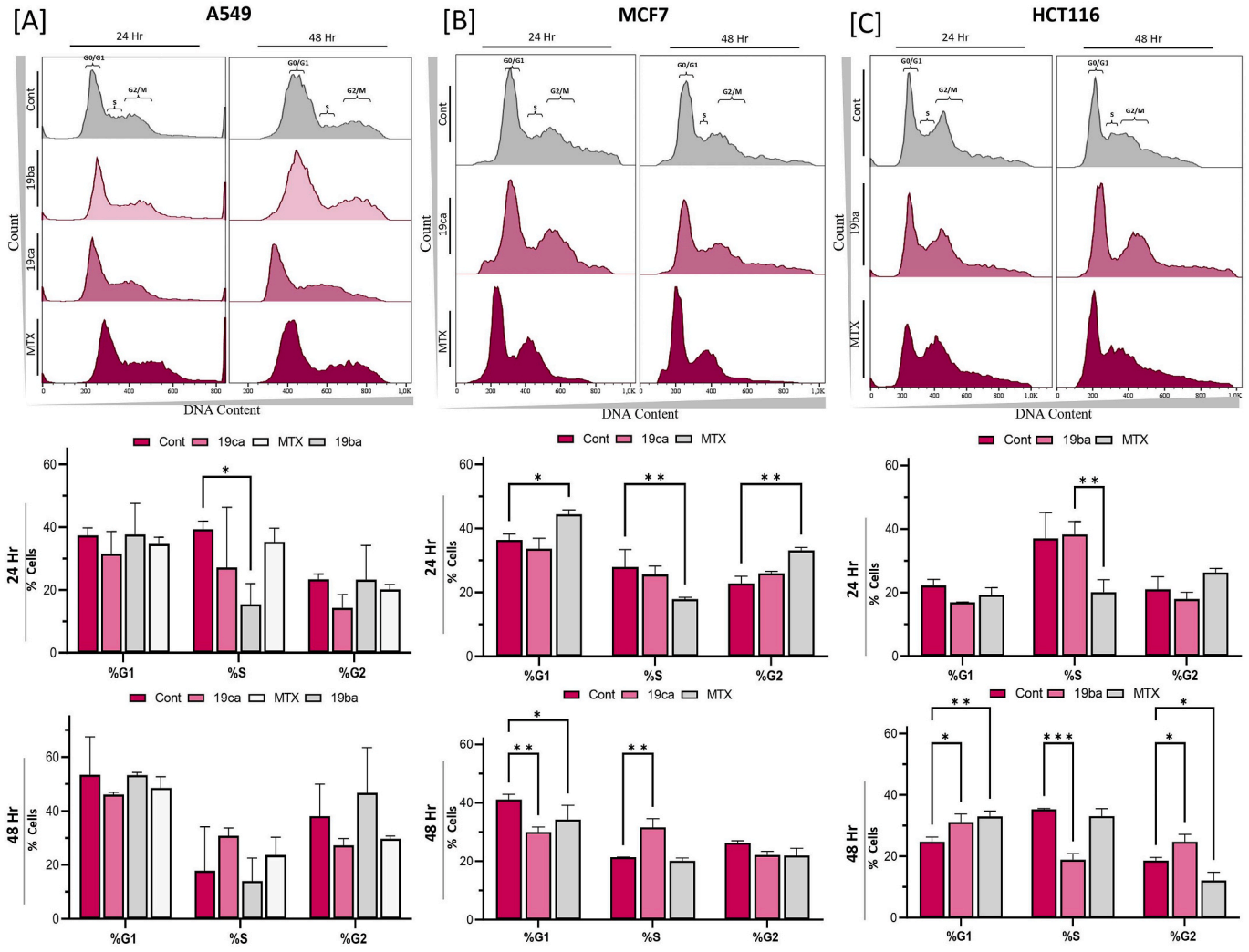

Fig. 4. The effects of selected compounds on cell cycle distribution in MCF-7, A549, and HCT116 cells and its quantitative analysis after compound treatment for 24 and 48 h at IC_{50} concentration. The statistical analysis was performed using a two-way ANOVA and Tukey's test. The data represent mean ± SD (n = 3). Significance levels are indicated as ns ($p > 0.05$), * ($p \leq 0.05$), ** ($p \leq 0.01$), and *** ($p \leq 0.001$).

about 4.56 ± 0.81 % to 6.56 ± 1.17 %. Compound (**19ba**) induced apoptosis from about 16.64 ± 3.81 % at 24 h to 27.97 ± 2.10 % at 48 h, while (**19ca**) more than doubled the apoptotic rate from 20.75 ± 3.81 % to 42.87 ± 1.07 %. MTX showed high initial apoptosis at 30.26 ± 2.84 % at 24 h and remained nearly constant at 32.27 ± 2.15 % at 48 h (Fig. 8B and E). In HCT116 cells, control apoptosis was nearly stable around 8.10 ± 2.16 % and 6.82 ± 1.05 % at 24 and 48 h, respectively. However, (**19ba**) exhibited a dramatic increase in apoptotic cells, from 17.50 ± 1.56 % to 45.03 ± 4.62 %. MTX induced high apoptosis at 32.01 ± 2.01 % at 24 h and slightly decreased to 31.10 ± 3.43 % at 48 h (Fig. 8A and D). The MCF-7 cell line showed a gradual increase in control apoptosis from 5.70 ± 1.56 % to 7.53 ± 1.16 %. The impact of (**19ca**) was remarkable, increasing from 10.80 ± 0.98 % at 24 h to a prominent 47.28 ± 4.15 % at 48 h. MTX also had a significant effect, showing an increase from 11.55 ± 2.01 % to 67.63 ± 3.26 %, indicating a remarkable apoptotic response (Fig. 8C and F). These observations suggest that (**19ca**) and MTX are particularly effective in inducing apoptosis in cancer cells, with compound-specific responses varying across different cell lines and time points. The data indicate that the apoptotic effect of MTX is prominent across all tested cell lines, while the effects of novel compounds like (**19ba**) and (**19ca**) show variable efficacy, which may depend on the specific cellular contexts of A549, HCT116, and MCF-7 cells. This analysis provides a foundation for further exploration of these compounds in cancer treatment research, with an emphasis on understanding the mechanisms behind their differential effects across various cancer cell types.

*2.1.1.7. Ex ovo angiogenesis and anti-tumorigenic effect of (**19ca**) and (**19ba**).* CAM assay was utilized to investigate the initial toxicity of novel compounds, specifically (**19ba**) and (**19ca**), on embryo development. This was conducted using an ex-ovo CAM model, where toxicity assessments were made at the early stage of incubation (day 6). The findings revealed that compound (**19ba**) exhibits significant embryotoxicity at nanomolar concentrations. However, at optimized concentrations of 1.5 μM/CAM and 4.5 μM/CAM, embryo survival rates ranged between 70 and 80 % (Fig. 9C). Due to its high toxicity, further *ex-ovo* experiments with compound (**19ba**) have been discontinued. Conversely, the experiments conducted with compound (**19ca**) focused on its effects on angiogenesis and tumor growth. These studies were performed on CAMs developed over 7 days, with observations recorded at 24 and 48 h. The results, as shown in (Fig. 9A–B), indicated a time-dependent reduction in blood vessel formation, assessed by counting the branching points of blood vessels. Moreover, dose-dependent studies demonstrated that (**19ca**) significantly reduced the size of tumors developed on the CAM, which are detailed in Fig. 9D–E. Further histological analyses using Hematoxylin and Eosin (H&E) staining provided

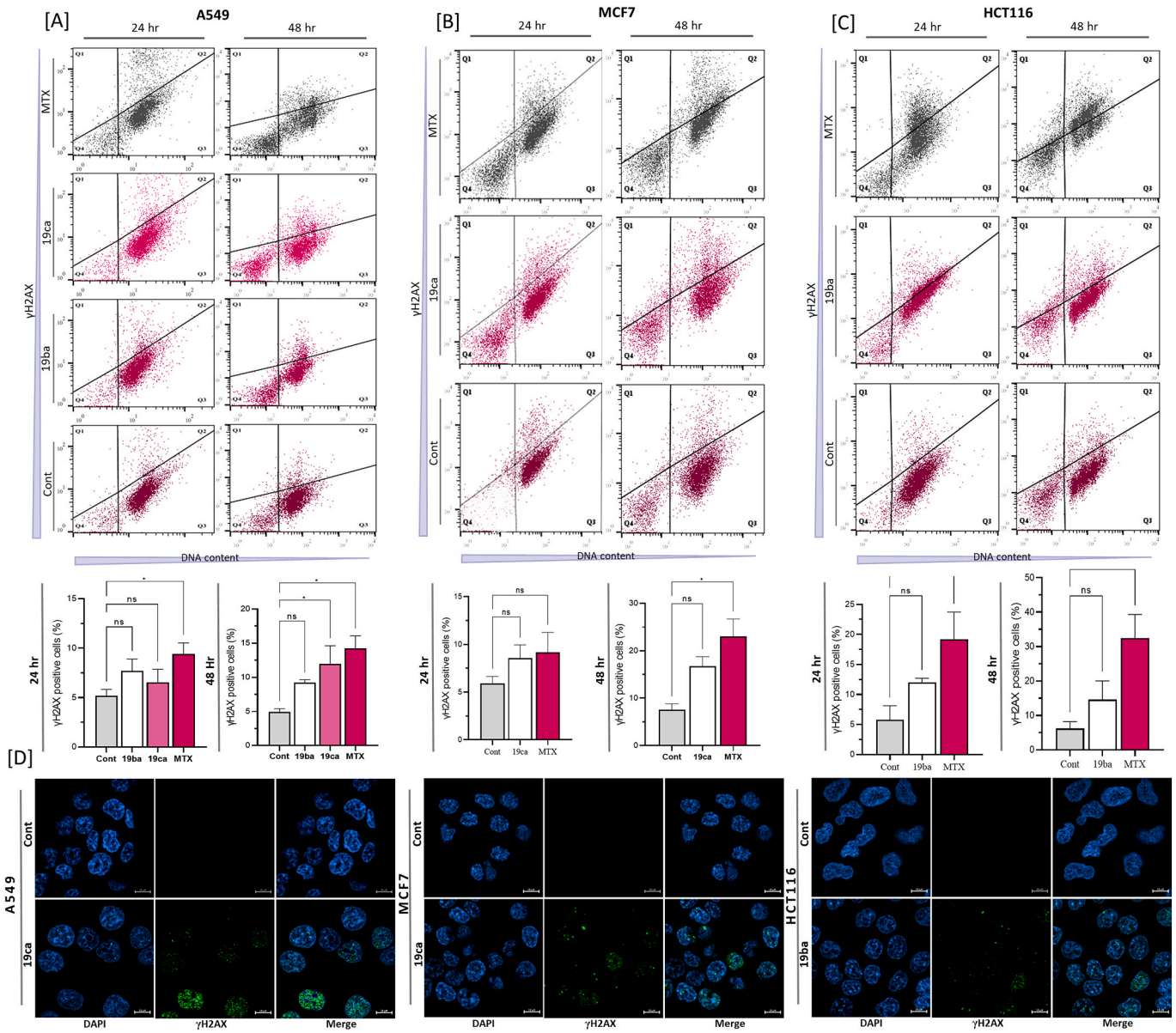

Fig. 5. Panels (**A**)–(**C**) depict the flow cytometric evaluation of γH2AX presence in MCF-7, A549, and HCT116 cell lines following treatment with compounds (**19ba**) and (**19ca**) at IC_{50} concentrations over 24 and 48 h, accompanied by quantitative analysis of the results. Panel (**D**) presents confocal microscopy images showing γH2AX foci within the treated cells. Statistical significance was determined using two-way ANOVA followed by Tukey's post-hoc test. Data are expressed as mean ± SD (n = 3). Significance levels are indicated as ns ($p > 0.05$), * ($p \leq 0.05$), ** ($p \leq 0.01$), and *** ($p \leq 0.001$).

additional insights into the morphological impacts of (**19ca**) on tumor cells. (Fig. 9F) illustrates a longitudinal section of the CAM, highlighting its normal vascular and epithelial appearance. (Fig. 9G–H) depict microtumors formed from A549 and MCF-7 cell lines on the CAM, treated with (**19ca**). These images reveal signs of necrosis and changes in nuclear morphology in some cells, underscoring the potential anti-tumorigenic effects of compound (**19ca**). These findings here also underscore the usefulness of the CAM assay in preclinical drug development. The model's ability to mimic human tumor microenvironments, along with its ethical and economic benefits, makes it a valuable tool for initial toxicity screening and mechanistic studies of novel therapeutics. Insights gained from studies like these not only advance our understanding of compound actions but also guide subsequent *ex-ovo* experiments aimed at developing effective anti-cancer drugs.

3. Experimental section

3.1. Materials and methods (chemistry)

Commercially available reagents were purchased from Sigma-Aldrich or Acros. Thin Layer Chromatography (TLC) analysis was performed on aluminum gel plates SiliaPlate SILICYCLE UltraPure and visualized with a UV lamp with a wavelength of 254 nm. Purification was performed using the BUCHI Pure C-815 flash chromatograph. FlashPure ID cartridges (silica 40 μm irregular) were used during the purification process. ^{1}H and ^{13}C NMR spectra were recorded on a Varian INOVA 500 spectrometer at 500 MHz and 125 MHz, respectively. NMR chemical shifts were reported in δ (ppm) using residual solvent peaks as standards, with the coupling constant J measured in Hz. High-resolution mass spectra were recorded with an Agilent 6540 Q-TOF system. HPLC analysis was performed using the liquid chromatograph Agilent Infinity II (1260 series) equipped with: quaternary pump (G7111A),

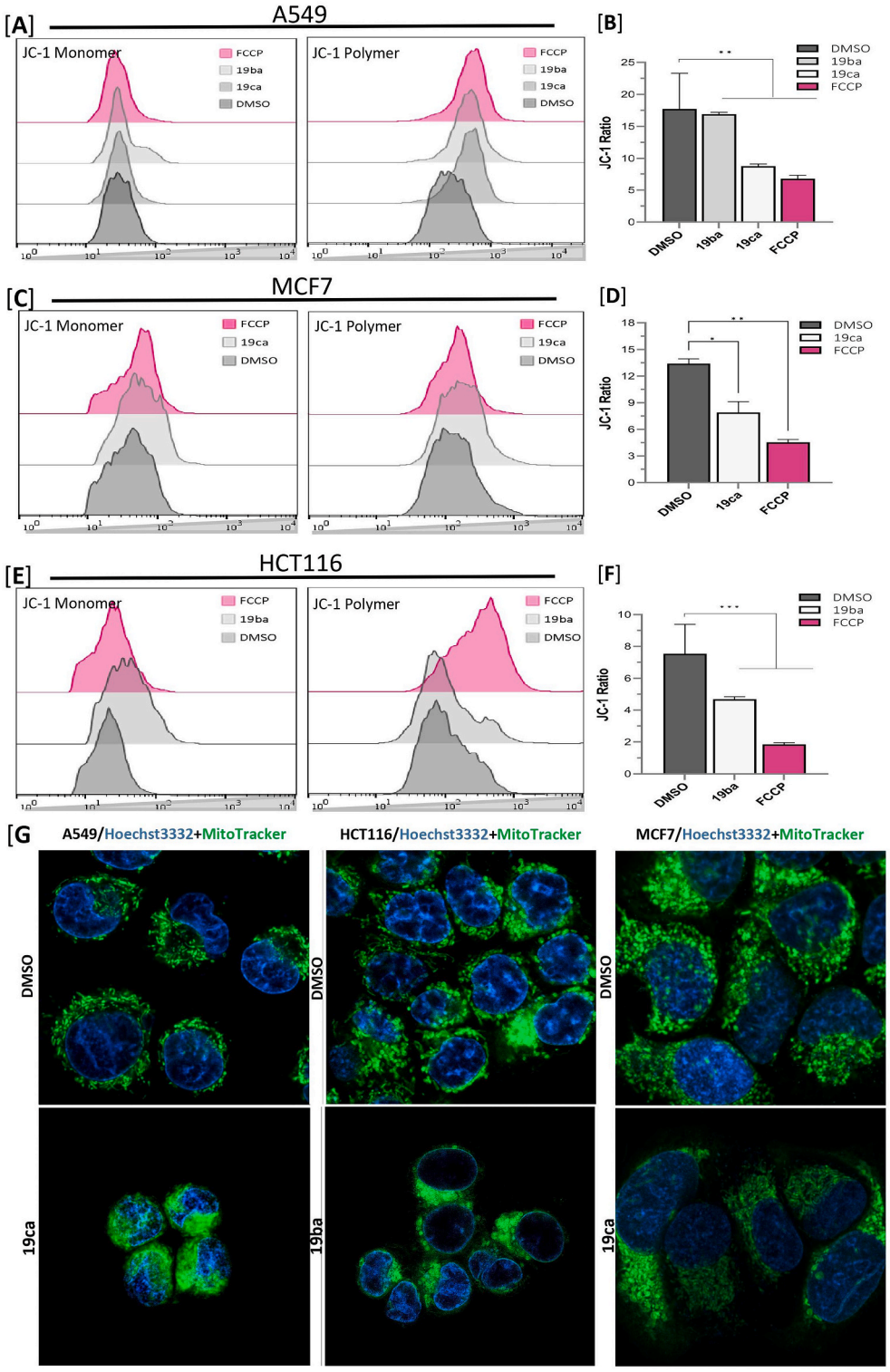

Fig. 6. Panels (**A**)–(**F**) represents Flow cytometric analyses of ΔΨm using JC-1 staining of A549, MCF-7, HCT116 and their respective quantification of JC-1 ratio (J-aggregates/J-monomers). Panels (**G**) represents the representative confocal microscopic image for (**19ba**) in HCT116 and (**19ca**) in A549 and MCF-7 respectively. Statistical significance was determined using two-way ANOVA followed by Tukey's post-hoc test. Data are expressed as mean ± SD (n = 3). Significance levels are indicated as ns ($p > 0.05$), * ($p \leq 0.05$), ** ($p \leq 0.01$), and *** ($p \leq 0.001$).

multicolumn thermostat (G7116A), and diode array UV detector (G7115A). Chromatographic analyzes were performed in the reversed phase system with column Poroshell 120 EC-C18 (100 x 4,6 mm, 4 μm). Mobile phases A: water B: ACN. The elution isocrat program was used with B = 80 % within 4 min; stop time 4 min; Column temperature 30 °C, 20 μL injection, Solvent flow 1.0 mL/min, UV detection at 254 nm; All compounds are >95 % pure by HPLC analysis.

3.2. *General procedure (a): closing the tetrahydrocarbazole scaffold (fischer indolization) (17aa-17ab)*

A-bottom flask (10 mL) is placed in an oil bath (liquid paraffin) on a

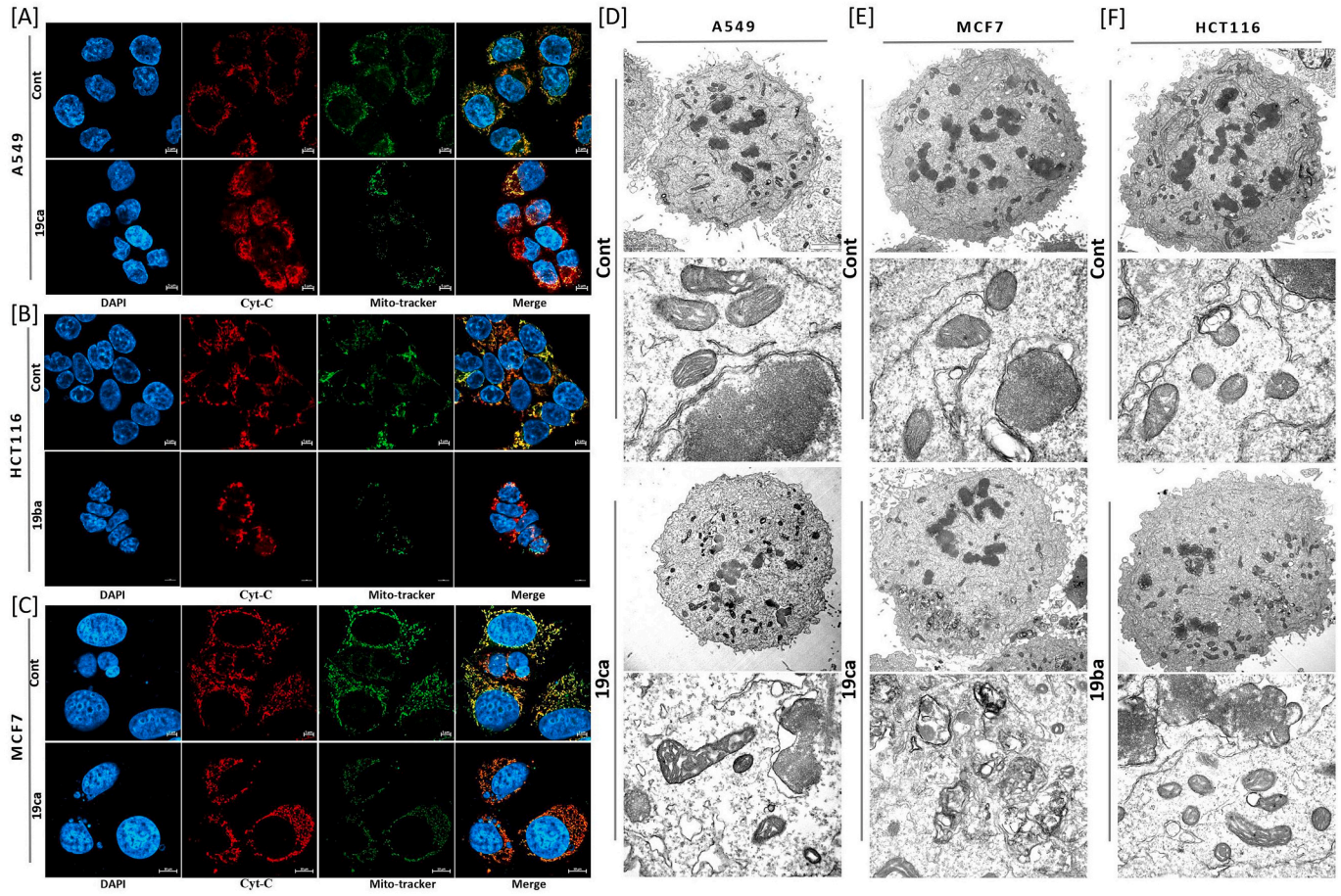

Fig. 7. Panels (**A**)–(**C**) show confocal microscopy images of A549, HCT116, and MCF-7 cells treated with compounds (**19ba**) and (**19ca**) at IC_{50} concentrations for 48 h. Panels (**D**)–(**F**) display TEM images of the same cell lines following treatment with the tested compounds.

magnetic stirrer under a reflux condenser in an argon atmosphere. (1.0 mmol) of phenylhydrazine hydrochloride (**15**) and (1.0 mmol) of cyclohexanone (**16**) are added and dissolved in anhydrous EtOH (5 mL). The reactions are carried out at the boiling point of the solvent at 79 °C for 24 h. The crude product is purified by flash chromatography using a solvent system.

3.3. N,N'-(2,3,4,9-tetrahydro-1H-carbazole-3,6-diyl)diacetamide (17aa)

Purification by flash column chromatography (DCM/MeOH, 10:1); form: white amorphous solid; yield: 35 %; **^{1}H NMR (500 MHz) (DMSO-d_6) δ=** 10.59 (s, **1H**), 9.66 (s, **1H**), 7.94 (d, *J* = 7.5 Hz, **1H**), 7.58 (s, **1H**), 7.12 (d, *J* = 8.5 Hz, **1H**), 7.09 (dd, *J* = 9 Hz, *J* = 2 Hz, **1H**), 3.37-3.32 (m, **1H**), 2.85-2.79 (m, **1H**), 2.77-2.72 (m, **2H**), 2.45-2.38 (m, **1H**), 1.99 (s, **3H**), 1.97-1.94 (m, **1H**), 1.81 (s, **3H**), 1.76-1.70 (m, **1H**); **^{13}C NMR (125 MHz) (DMSO-d_6) δ=** 169.08, 167.88, 134.73, 133.27, 131.32, 127.34, 114.31, 110.70, 108.46, 106.83, 60.19, 45.60, 29.04, 27.69, 24.33, 23.23; **(ESI+): m/z [M + H]$^+$** calcd for $C_{16}H_{19}N_3O_2$, 285.15; found, 286.1565. **HPLC RT** = 0.958 min, Area = 99.90 % (254 nm)

3.4. N-(6-(trifluoromethoxy)-2,3,4,9-tetrahydro-1H-carbazol-3-yl) acetamide (17ba)

Purification by flash column chromatography (DCM/MeOH, 20:1); form: white amorphous solid; yield: 77 %; **^{1}H NMR (500 MHz) (acetone-d_6) δ=** 10.27 (s, **1H**), 7.39 (d, *J* = 7.5 Hz, **1H**), 7.36 (d, *J* = 9.0 Hz, **1H**), 7.29 (s, **1H**), 7.97 (dd, *J* = 8.5 Hz, *J* = 1 Hz, **1H**), 4.31-4.24 (m, **1H**), 3.03-2.98 (m, **1H**), 2.88-2.83 (m, **2H**), 2.60-2.54 (m, **1H**), 2.09-2.06 (m, **1H**), 1.97-1.92 (m, **1H**), 1.90 (s, **3H**); **^{13}C NMR (125 MHz) (acetone-d_6) δ=** 168.99, 142.15, 136.21, 135.08, 127.94, 121.0 (q, $^kJ_{CF}$ = 252.5 Hz), 113.93, 111.24, 109.73, 107.63, 45.11, 28.25, 27.08, 22.12, 20.83; **(ESI+): m/z [M + H]$^+$** calcd for $C_{15}H_{15}F_3N_2O_2$, 312.11; found, 313.1158.

3.5. N-(6-bromo-2,3,4,9-tetrahydro-1H-carbazol-3-yl)acetamide (17ca)

Purification by flash column chromatography (DCM/MeOH, 20:1); form: white amorphous solid; yield: 47 %; **^{1}H NMR (500 MHz) ($CDCl_3$) δ=** 7.95 (s, **1H**), 7.55 (d, *J* = 2.5 Hz, **1H**), 7.24 (dd, *J* = 10.5 Hz, *J* = 2.0 Hz, **1H**), 7.18 (d, *J* = 10.5 Hz, **1H**), 5.63 (s, **1H**), 3.09-3.01 (m, **1H**), 2.92-2.76 (m, **2H**), 2.61-2.53 (m, **1H**), 2.16-2.09 (m, **1H**), 2.00 (s, **3H**), 1.71-1.61 (m, **1H**); **^{13}C NMR (125 MHz) ($CDCl_3$) δ=** 169.72, 134.76, 134.26, 129.37, 124.24, 120.41, 112.65, 111.92, 107.17, 45.07, 27.92, 27.54, 23.58, 20.56; **(ESI+): m/z [M + H]$^+$** calcd for $C_{14}H_{15}BrN_2O$, 306.04; found, 307.0045.

3.6. N-(6-sulfamoyl-2,3,4,9-tetrahydro-1H-carbazol-3-yl)acetamide (17da)

Purification by flash column chromatography (DCM/MeOH, 20:1); form: white amorphous solid; yield: 67 %; **^{1}H NMR (500 MHz) (acetone-d_6) δ=** 11.21 (s, **1H**), 7.98 (d, *J* = 7.5 Hz, **1H**), 7.83 (s, **1H**), 7.50 (dd, *J* = 8.5 Hz, *J* = 1.5 Hz, **1H**), 7.37 (d, *J* = 8.5 Hz, **1H**), 7.10-7.03 (m, **2H**), 4.10-4.02 (m, **1H**), 2.96-2.89 (m, **1H**), 2.84-2.78 (m, **2H**), 2.56-2.48 (m, **1H**), 2.02-1.95 (m, **1H**), 1.82 (s, **3H**), 1.80-1.75 (m, **1H**); **^{13}C NMR (125 MHz) (acetone-d_6) δ=** 169.24, 137.79, 136.64, 134.64,

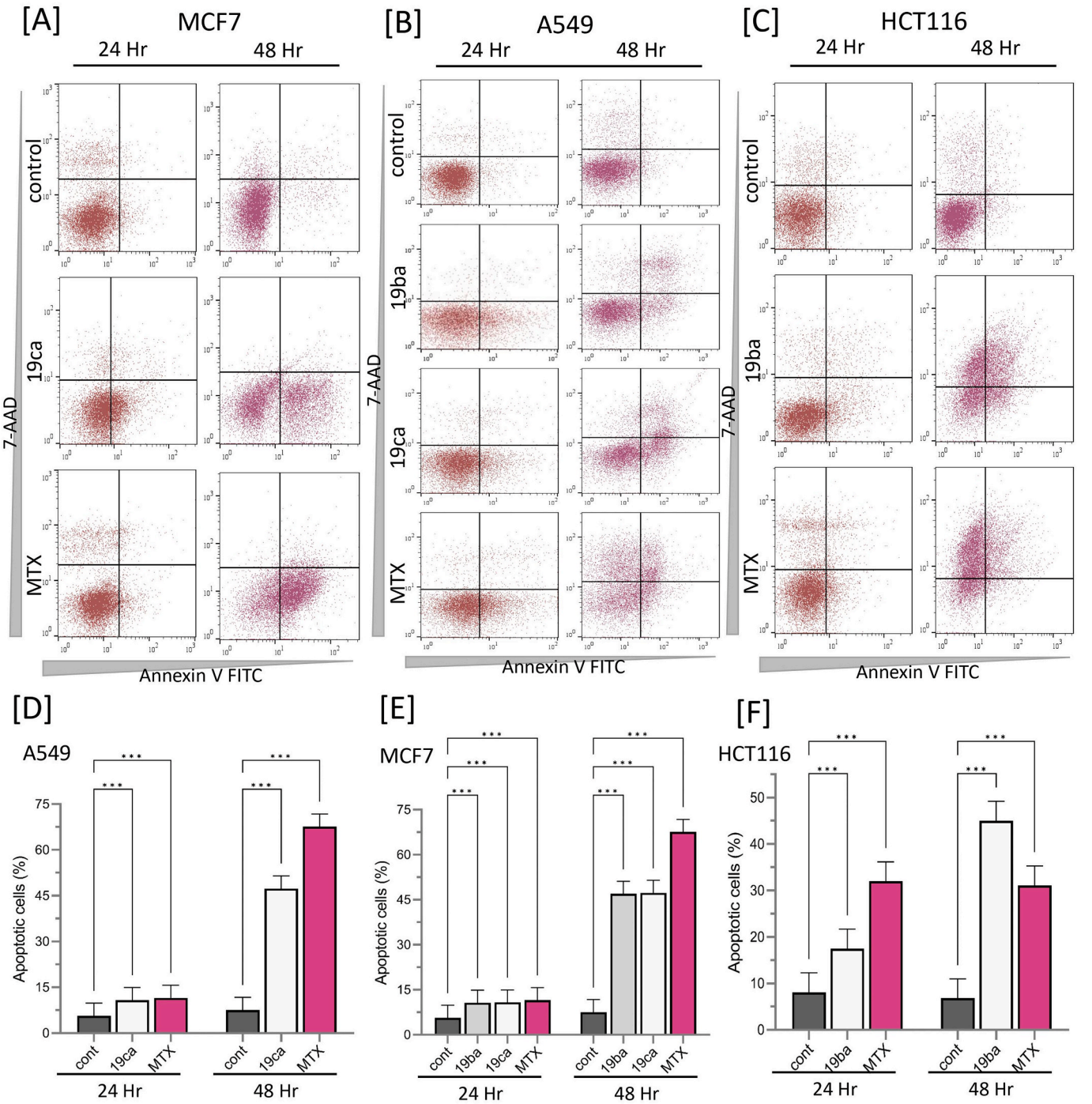

Fig. 8. Induction of apoptosis in various cancer cell lines by compounds (**19ba**) and (**19ca**), assessed through flow cytometry. Panels (**A**), (**B**), and (**C**) display results for MCF-7, A549, and HCT116 cell lines, respectively. Quantitative analysis involved two-way ANOVA and Tukey's post-hoc test. Data are presented as mean ± SD for three independent experiments; significance levels are denoted as ns ($p > 0.05$), * ($p \leq 0.05$), ** ($p \leq 0.01$), and *** ($p \leq 0.001$).

126.61, 118.37, 115.96, 111.02, 108.15, 45.31, 28.69, 27.34, 23.22, 21.40; **(ESI+): m/z [M + H]** $^{+}$ calcd for $C_{14}H_{17}N_3O_3S$, 307.10; found, 308.1065. **HPLC RT** = 0.952 min, Area = 97.12 % (254 nm)

3.7. Tert-butyl (6-acetamido-2,3,4,9-tetrahydro-1H-carbazol-3-yl) carbamate (17 ab)

Purification by flash column chromatography (AcOEt/Hexanes, 3:1, 1 % Et_3N)); form: white amorphous solid; yield: 91 %; **^{1}H NMR (500 MHz) (DMSO-d_6) δ**= 10.57 (s, **1H**), 9.65 (s, **1H**), 7.61 (s, **1H**), 7.14 (d, *J* = 9.5 Hz, **1H**), 7.09 (dd, *J* = 10.5 Hz, *J* = 2 Hz, **1H**), 6.96 (d, *J* = 9.5 Hz, **1H**), 3.77-3.65 (m, **1H**), 2.87-2.79 (m, **1H**), 2.77-2.71 (m, **2H**), 2.48-2.38 (m, **1H**), 2.01 (s, **3H**), 1.75-1.65 (m, **1H**), 1.41 (s, **9H**), 1.34-1.24 (m, **1H**); **^{13}C NMR (125 MHz) (DMSO-d_6) δ**= 167.88, 155.54, 134.73, 133.31, 131.34, 127.31, 114.22, 110.72, 108.40, 107.10, 77.97, 60.22, 47.45, 29.64, 28.78, 27.85, 24.38, 22.08, 21.23; **(ESI+): m/z [M + H]** $^{+}$ calcd for $C_{19}H_{25}N_3O_3$, 343.19; found, 344.1970. **HPLC RT** = 1.098 min, Area = 96.51 % (254 nm)

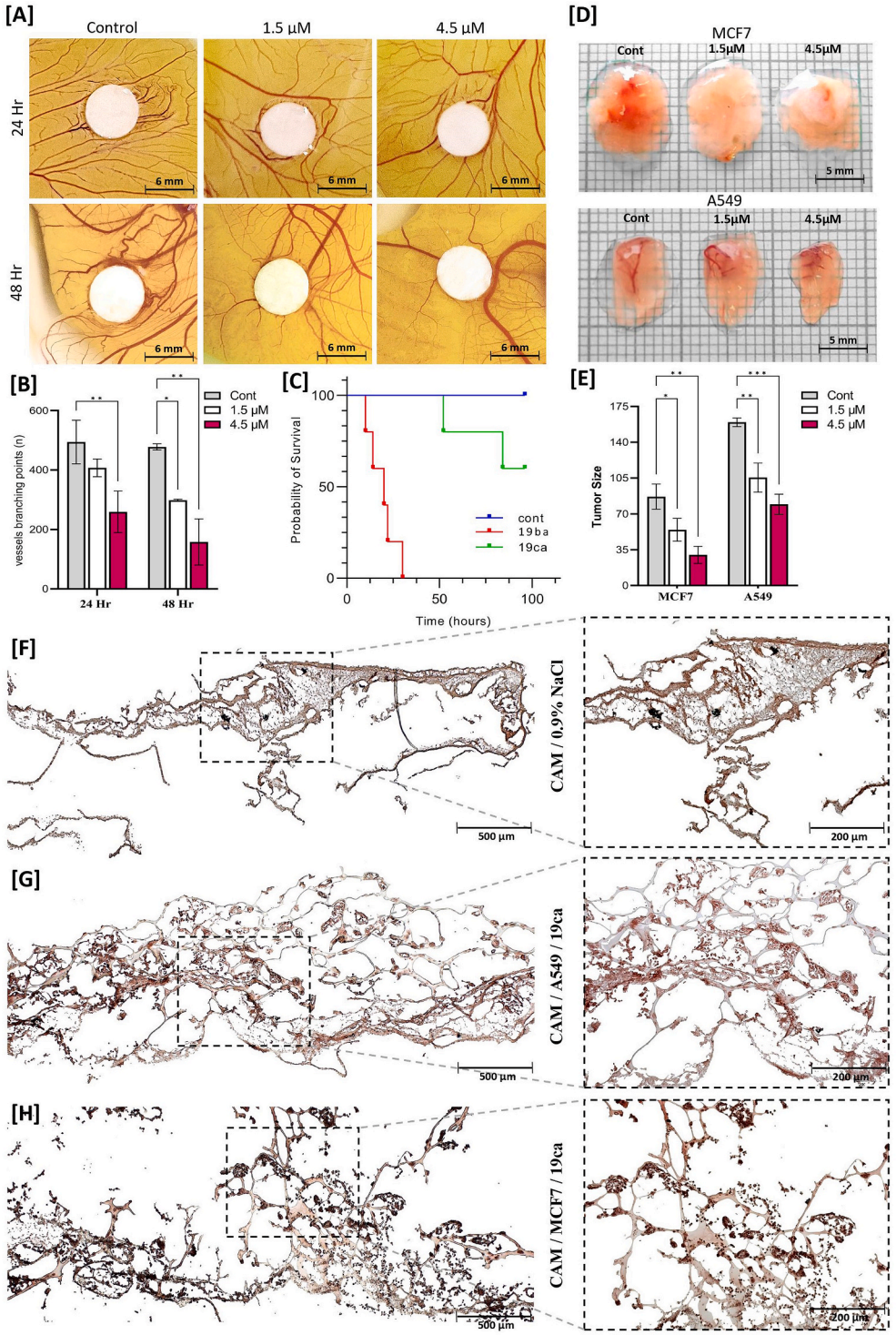

Fig. 9. Panels (**A**) represents the effect of angiogenic inhibitory potential of (**19ca**) on CAM and (**B**) its quantification in terms of branching points. (**C**) Kaplan Mayer survival analysis of compounds (**19ba**) and (**19ca**). (**D**) A549 and MCF-7 tumor cell xenograft on cam with respect to test compound treatment (**E**) its quantification in terms of tumor size. Panels (**F–H**) H&E staining of tumors from (Fig. 9D).

*3.8. **General procedure (b) and (c):** removal of BOC protection and acylation reaction (**18aa-18af**)*

tert-butyl (6-acetamido-2,3,4,9-tetrahydro-1H-carbazol-3-yl)carbamate (100 mg, 0.3 mmol), TFA (1.25 mL) and DCM (2.5 mL) were added to a round-bottom flask placed on a magnetic stirrer. The reactions were carried out at room temperature for 1 h. The progress of the reaction was monitored by TLC in a solvent system (3:1, A:H + 1 % Et_3N). The solvent was evaporated and the crude product was used for the next step. Salt 6-acetamido-2,3,4,9-tetrahydro-1H-carbazol-3-aminium, organic carboxylic acid R^3COOH (0.3 mmol), TBTU (105 mg, 0.3 mmol), DMF (7 mL) and TEA (1.2 mL) were added to a round-bottom flask on a magnetic stirrer. The reactions were carried out at room temperature for 24 h. DMF was evaporated and extractions were performed. DCM (20 mL) was added to the reaction mixture, then the organic layer was washed with 10 % citric acid (2 mL), then sodium bicarbonate (2 mL). The mixture

was left with the drying agent. The magnesium sulfate was filtered off, and the mixture was concentrated on a rotary evaporator. The crude product was purified using flash chromatography.

3.9. N-(6-acetamido-2,3,4,9-tetrahydro-1H-carbazol-3-yl)benzamide (18aa)

Purification by flash column chromatography (AcOEt 100 %); form: white amorphous solid; yield: 67 %; **^{1}H NMR (500 MHz) (DMSO-d_6) δ=** 10.62 (s, **1H**), 9.66 (s, **1H**), 8.46 (d, *J* = 8.0 Hz, **1H**), 7.90-7.40 (m, **5H -Ph**), 7.61 (s, 1H), 7.13 (d, *J* = 8.5 Hz, **1H**), 7.09 (dd, *J* = 8.5 Hz, *J* = 1.5 Hz, **1H**), 4.30-4.18 (m, **1H**), 2.94-2.90 (m, **1H**), 2.86-2.78 (m, **2H**), 2.66-2.58 (m, **1H**), 2.12-2.04 (m, **1H**), 1.99 (s, 3H), 1.92-1.84 (m, **1H**); **^{13}C NMR (125 MHz) (DMSO-d_6) δ=** 167.89, 166.31, 135.23, 134.76, 133.30, 131.49, 131.35, 128.62, 127.77, 127.27, 114.27, 110.75, 108.41, 107.15, 60.21, 46.79, 29.41, 27.60, 24.35, 22.33, 21.22; **(ESI+): m/z [M + H]$^+$** calcd for C21H21N3O2, 347.16; found, 348.1718. **HPLC RT** = 1.021 min, Area = 99.56 % (254 nm)

3.10. N-(6-acetamido-2,3,4,9-tetrahydro-1H-carbazol-3-yl)-5-methylfuran-2-carboxamide (18 ab)

Purification by flash column chromatography (AcOEt 100 %); form: white amorphous solid; yield: 85 %; **^{1}H NMR (500 MHz) (DMSO-d_6) δ=** 10.60 (s, **1H**), 9.65 (s, **1H**), 8.18 (d, *J* = 8.0 Hz, **1H**), 7.57 (s, **1H**), 7.12 (d, *J* = 8.5 Hz, **1H**), 7.09 (dd, *J* = 8.5 Hz, *J* = 1.5 Hz, **1H**), 7.00 (d, *J* = 3.5 Hz, **1H**), 6.22 (d, *J* = 2.5 Hz, **1H**), 4.22-4.12 (m, **1H**), 2.86-2.80 (m, **1H**), 2.80-2.72 (m, **2H**), 2.64-2.58 (m, **1H**), 2.32 (s, **3H**), 2.05-2.01 (m, **1H**), 1.98 (s, **3H**), 1.93-1.83 (m, **1H**); **^{13}C NMR (125 MHz) (DMSO-d_6) δ=** 167.89, 157.75, 154.50, 147.01, 134.70, 133.30, 131.34, 127.23, 114.87, 114.33, 110.75, 108.55, 108.43, 107.09, 46.01, 29.37, 27.58, 24.34, 22.28, 21.22; **(ESI+): m/z [M + H]$^+$** calcd for $C_{20}H_{21}N_3O_3$, 351.16; found, 352.1673. **HPLC RT** = 1.013 min, Area = 100.00 % (254 nm)

3.11. N-(6-acetamido-2,3,4,9-tetrahydro-1H-carbazol-3-yl)-5-ethylfuran-2-carboxamide (18ac)

Purification by flash column chromatography (AcOEt 100 %); form: white amorphous solid; yield: 81 %; **^{1}H NMR (500 MHz) (DMSO-d_6) δ=** 10.60 (s, **1H**), 9.65 (s, **1H**), 8.18 (d, *J* = 8.0 Hz, **1H**), 7.58 (s, **1H**), 7.13 (d, *J* = 8.5 Hz, **1H**), 7.10 (dd, *J* = 8.5 Hz, *J* = 2.0 Hz, **1H**), 7.02 (d, *J* = 3.0 Hz, **1H**), 6.23 (d, *J* = 3.5 Hz, **1H**), 4.21-4.13 (m, **1H**), 2.84-2.80 (m, **1H**), 2.80-2.77 (m, **2H**), 2.66 (q, *J* = 7.5 Hz, **2H**), 2.64-2.58 (m, **1H**), 2.06-2.00 (m, **1H**), 1.98 (s, **3H**), 1.94-1.82 (m, **1H**), 1.19 (q, *J* = 8.0 Hz, **3H**); **^{13}C NMR (125 MHz) (DMSO-d_6) δ=** 167.89, 159.87, 157.82, 146.85, 134.71, 133.30, 131.34, 127.23, 114.66, 114.33, 110.75, 108.43, 107.10, 107.01, 46.06, 31.15, 29.41, 27.61, 24.34, 22.32, 21.39; **(ESI+): m/z [M + H]$^+$** calcd for $C_{21}H_{23}N_3O_3$, 365.17; found, 366.1817. **HPLC RT** = 1.044 min, Area = 99.87 % (254 nm)

3.12. N-(6-acetamido-2,3,4,9-tetrahydro-1H-carbazol-3-yl)-5-bromofuran-2-carboxamide (18ad)

Purification by flash column chromatography (AcOEt 100 %); form: white amorphous solid; yield: 79 %;

^{1}H NMR (500 MHz) (DMSO-d_6) δ= 10.61 (s, **1H**), 9.65 (s, **1H**), 8.45 (d, *J* = 7.5 Hz, **1H**), 7.58 (s, **1H**), 7.17 (d, *J* = 3.5 Hz, **1H**), 7.13 (d, *J* = 8.5 Hz, **1H**), 7.10 (dd, *J* = 8.5 Hz, *J* = 1.5 Hz, **1H**), 6.73 (d, *J* = 3.5 Hz, **1H**), 4.22-4.12 (m, **1H**), 2.87-2.81 (m, **1H**), 2.80-2.73 (m, **2H**), 2.67-2.57 (m, **1H**), 2.06-2.01 (m, **1H**), 1.99 (s, **3H**), 1.93-1.83 (m, **1H**); **^{13}C NMR (125 MHz) (DMSO-d_6) δ=** 167.90, 156.64, 150.29, 134.68, 133.30, 131.35, 127.20, 124.68, 116.26, 114.36, 110.76, 108.42, 106.99, 46.29, 29.28, 27.48, 24.34, 22.27, 21.21; **(ESI+): m/z [M + H]$^+$** calcd for $C_{19}H_{18}BrN_3O_3$, 415.05; found, 416.0604. **HPLC RT** = 1.041 min, Area = 100.00 % (254 nm)

3.13. N-(6-acetamido-2,3,4,9-tetrahydro-1H-carbazol-3-yl)-5-methylthiophene-2-carboxamide (18ae)

Purification by flash column chromatography (AcOEt 100 %); form: white amorphous solid; yield: 96 %; **^{1}H NMR (500 MHz) (DMSO-d_6) δ=** 10.61 (s, **1H**), 9.65 (s, **1H**), 8.34 (d, *J* = 8.0 Hz, **1H**), 7.62 (d, *J* = 3.5 Hz, **1H**), 7.60 (s, **1H**), 7.13 (d, *J* = 9.0 Hz, **1H**), 7.09 (dd, *J* = 8.5 Hz, *J* = 1.5 Hz, **1H**), 6.82 (d, *J* = 4.5 Hz, **1H**), 4.21-4.11 (m, **1H**), 2.91-2.85 (m, **1H**), 2.83-2.75 (m, **2H**), 2.63-2.55 (m, **1H**), 2.44 (s, **3H**), 2.09-2.03 (m, **1H**), 1.99 (s, **3H**), 1.90-1.81 (m, **1H**); **^{13}C NMR (125 MHz) (DMSO-d_6) δ=** 167.89, 161.08, 144.83, 138.24, 134.73, 133.30, 131.36, 128.63, 127.24, 126.71, 114.32, 110.75, 108.43, 107.06, 46.69, 29.50, 27.69, 24.35, 22.30, 21.21; **(ESI+): m/z [M + H]$^+$** calcd for $C_{20}H_{21}N_3O_2S$, 367.14; found, 368.1427. **HPLC RT** = 1.045 min, Area = 94.27 % (254 nm)

3.14. N-(6-acetamido-2,3,4,9-tetrahydro-1H-carbazol-3-yl)-1H-indole-2-carboxamide (18af)

Purification by flash column chromatography (AcOEt 100 %) form: white amorphous solid; yield: 30 %; **^{1}H NMR (500 MHz) (DMSO-d_6) δ=** 11.56 (s, **1H**), 10.63 (s, **1H**), 9.66 (s, **1H**), 8.45 (d, *J* = 8.0 Hz, **1H**), 7.60 (s, **1H**), 7.59 (d, *J* = 8.5 Hz, **1H**), 7.41 (d, *J* = 8.0 Hz, **1H**), 7.20-6.99 (m, **5H**), 4.31-4.21 (m, **1H**), 2.96-2.90 (m, **1H**), 2.86-2.81 (m, **2H**), 2.67-2.60 (m, **1H**), 2.15-2.04 (m, **1H**), 1.99 (s, **3H**), 1.94-1.86 (m, **1H**); **^{13}C NMR (125 MHz) (DMSO-d_6) δ=** 167.90, 161.04, 136.81, 134.78, 133.32, 132.34, 131.36, 127.51, 127.27, 123.64, 121.88, 120.09, 114.32, 112.70, 110.76, 108.44, 107.03, 103.14, 46.40, 31.15, 29.44, 27.74, 24.35; **(ESI+): m/z [M + H]$^+$** calcd for $C_{23}H_{22}N_4O_2$, 386.17; found, 387.1807. **HPLC RT** = 1.052 min, Area = 99.75 % (254 nm)

3.15. General procedure (d): thionation (19ba-19ca)

N-(6-bromo/trifluoromethoxy-2,3,4,9-tetrahydro-1H-carbazol-3-yl) acetamide (0.16 mmol), P_2S_5 (0.33 mmol) and anhydrous dioxane (13.2 mL) were placed in a round-bottom flask. The solution was stirred at room temperature for 72 h. The solvent was then evaporated. The mixture was diluted with $NaHCO_3$ (2 mL) and then extracted with ethyl acetate (3x5mL). The organic layer was dried over $MgSO_4$. The drying agent was filtered off and flash chromatography was performed.

3.16. N-(6-(trifluoromethoxy)-2,3,4,9-tetrahydro-1H-carbazol-3-yl) acetamide (19ba)

Purification by flash column chromatography (DCM/MeOH, 10:1); form: white amorphous solid; yield: 60 %; **^{1}H NMR (500 MHz) (DMSO-d_6) δ=** 11.06 (s, **1H**), 10.07 (d, *J* = 7.5 Hz, **1H**), 7.30 (d, *J* = 9.0 Hz, **1H**), 7.29 (s, **1H**), 6.95 (dd, *J* = 8.5 Hz, *J* = 1 Hz, **1H**), 4.72-4.62 (m, **1H**), 3.09-3.01 (m, **1H**), 2.85-2.79 (m, **2H**), 2.60-2.52 (m, **1H**), 2.40 (s, **3H**), 2.12-2.06 (m, **1H**), 1.98-1.90 (m, **1H**); **^{13}C NMR (125 MHz) (DMSO-d_6) δ=** 168.99, 142.15, 136.21, 135.08, 127.94, 121.0 (q, $^1J_{CF}$ = 252.5 Hz), 114.15, 111.90, 110.10, 107.20, 51.78, 33.48, 27.22, 26.02, 21.55; **(ESI+): m/z [M + H]$^+$** calcd $C_{15}H_{15}F_3N_2OS$, 328.09; found, 329.0978. **HPLC RT** = 1.404 min, Area = 98.27 % (254 nm)

3.17. N-(6-bromo-2,3,4,9-tetrahydro-1H-carbazol-3-yl)acetamide (19ca)

Purification by flash column chromatography (DCM/MeOH, 70:1); form: white amorphous solid; yield: 56 %; **^{1}H NMR (500 MHz) (acetone-d_6) δ=** 10.09 (s, **1H**), 9.20 (s, **1H**), 7.53 (d, *J* = 2.0 Hz, **1H**), 7.27 (d, *J* = 10.5 Hz, **1H**), 7.15 (dd, *J* = 11.0 Hz, *J* = 2.5 Hz, **1H**), 4.96-4.86 (m, **1H**), 3.20-3.12 (m, **1H**), 2.92-2.86 (m, **2H**), 2.73-2.67 (m, **1H**), 2.47 (s, **3H**), 2.24-2.17 (m, **1H**), 2.16-2.11 (m, **1H**); **^{13}C NMR (125 MHz) (acetone-d_i) δ=** 199.67, 138.21, 135.39, 129.56, 123.14, 119.84, 112.34, 111.41, 106.54, 51.38, 32.92, 26.43, 25.73, 20.66; **(ESI+): m/z**

[M + H] $^{+}$ calcd for $C_{14}H_{15}BrN_2S$, 322.01; found, 323.0216. **HPLC RT** = 1.403 min, Area = 95.56 % (254 nm)

3.18. Cell culturing and maintenance

In this study, four distinct cell lines were employed, specifically: MCF-7 (breast adenocarcinoma, sourced from ATCC under catalog HTB-22), A549 (lung carcinoma, from ATCC, CRM-CCL-185), HCT116 (colorectal carcinoma, from ATCC, CCL-247EMT), and MRC-5 (normal lung fibroblast, from ATCC, CCL-171). The HCT116 cells were cultured in McCoy's 5A medium, enhanced with 10 % fetal bovine serum, 2 mM L-glutamine, and antibiotics including penicillin (62.6 μg/mL) and streptomycin (40 μg/mL). Both MCF-7 and A549 cell lines were maintained in RPMI-1640 medium with the same concentrations of fetal bovine serum, L-glutamine, and antibiotics as used for HCT116. The MRC5 cells were cultured in Eagle's Minimum Essential Medium supplemented with 10 % fetal bovine serum. All cultures were incubated under conditions of 5 % CO_2 and controlled humidity to maintain optimal growth environments.

3.19. Determination of cell viability

The viability of cells was determined by the MTT assay, using 3-(4,5-dimethylthiazol-2-yl)-2,5-diphenyltetrazolium bromide from Sigma-Aldrich. The cells were then added to 96-well culture plates and allowed to attach by overnight incubation. After 72 h of treatment, the cells were incubated with different concentrations of the test compounds. The solvent control used was 1 % DMSO from Merck. After the samples' treatment, a solution of MTT at a concentration of 0.4 mg/mL was added to each well and incubated for 2–3 h at 37 °C. After an incubation period of 4 h, the medium was removed, and 100 μL of DMSO was added to dissolve the formazan crystals. Then, the absorbance of the solution was read at a wavelength of 450 nm in an ASYS UVM340 microplate reader. The IC_{50} of each compound was calculated from the dose-response curves of relative cell survival against compound concentration by using the GraphPad Prism 9 software. The results of the relative consistency and precision were obtained from the average data of three independent experiments.

3.20. Morphological evaluation

All the cell lines were cultured in their respective recommended media in appropriate culture plates to ensure optimal growth conditions. The cells were allowed to adhere overnight to achieve confluency suitable for treatment. Subsequently, these cells were treated with the experimental compounds for a period of 48 h, allowing for adequate exposure to assess cytotoxic effects. Post-treatment, the cells were stained using Hoechst 33342 and Propidium Iodide (both from Sigma-Aldrich) to evaluate nuclear morphology and viability. The stained cells were then examined under a fluorescence microscope (Olympus BX53), which facilitated detailed visualization of apoptotic and necrotic cells. This methodological approach aligns with established protocols in cytotoxicity testing, ensuring the reliability and reproducibility of the experimental outcomes.

3.21. Colony formation assay

In this study, the respective cells were used following seeding densities of 1700, 1400, and 1200 cells per well in 6-well plates for HCT116, MCF-7, and A549, respectively. Cells plated directly onto the surfaces of plates were allowed to attach prior to treatment with a range of concentrations of experimental compounds for a 24-h period. Following this exposure, the medium was refreshed, and cells were further cultured for eight days. Finally, the cells underwent various preparation stages of this phase: the first was washing with PBS to eliminate any unreacted experimental compounds; secondly, fixing for 20 min with 99.5 % methanol to protect their structure. The fixed cells were stained with a 0.5 % crystal violet solution for 20 min and air-dried to facilitate colony enumeration. Then the effectiveness of the compounds on cell viability was quantitatively estimated by counting the colonies stained using a colony counter. The values obtained from the respective treatments were then compared with those of the untreated control samples to derive percentages of viable cells.

3.22. Cellular adhesion assay

Cellular adhesion experiments were conducted using agar molds prepared with the 3D Petri Dish® system from Microtissues®. Initially, agar was liquefied using normal saline, sterilized, and then cast into a 3D Petri Dish®. Upon solidification, the molds were rinsed with the appropriate media and positioned in 24-well plates. Cell adhesion was initiated and allowed to proceed for 20 min before additional medium containing various drug dilutions, was introduced. Live cell imaging was performed using an Olympus CellVivo Inverted Microscope. Measurements of each rod's length were quantified utilizing Olympus CellSens software.

3.23. Cell cycle analysis

This experiment aims to elucidate the cytostatic and cytotoxic profiles of these agents, thereby contributing to a nuanced understanding of their mechanisms of action and potential therapeutic uses. The cell lines HCT116, A549 and MCF-7 were grown at sub-confluency under standard conditions in complete media on appropriate culture plates. The cell lines were treated with a designated experimental compound post-overnight adhesion for evaluating the efficacy of the compound over a time course of 24 and 48 h. After the post-treatment period, cells were fixed using 75 % ice-cold ethanol and stored at −20 °C, ensuring that cell integrity is fit for further analysis. After fixation, the cells were subsequently washed twice with phosphate-buffered saline (PBS) and centrifuged to form a pellet. Fixed cells were then subsequently stained with 20 μg/μL propidium iodide (PI) and 50 μg/μL RNase A in PBS. This step was very crucial, since it allowed time for intercalation of the DNA content to check on the cell cycle phases. Staining was done at room temperature for 30 min, allowing sufficient time for the intercalation of PI and the DNA. Following the treatment of the cells, the distribution of the cell cycle was quantitated using an 8-Color flow cytometer (Merck Millipore) from Guava easyCyte, providing an advanced platform for the rapid and accurate analysis. The FlowJo v10 software was used for data analysis.

3.24. Evaluation of DNA DSBs induction

The cell lines HCT116, A549, and MCF-7 were cultured and seeded onto tissue culture plates, allowing them to adhere overnight. The following day, the cells were exposed to the experimental compounds for durations of 24 and 48 h. MTX (1 μM) was utilized as a reference compound. Subsequently, the cells were harvested through trypsinization, fixed in 75 % ethanol, and stored at −20 °C until further analysis. To prepare the cells for analysis, they were rehydrated with PBS while placed on ice for 5 min. Following this, the cells were permeabilized with a solution consisting of 0.2 % Triton X-100 in PBS and incubated at room temperature for 15 min. For labelling purposes, the cells were treated with Alexa Fluor 488-conjugated mouse anti-p-γH2AX (Ser139) antibody (#613406, BioLegend, USA) at a dilution of 1:200, and incubated at 37 °C for 1.5 h. Afterwards, the cells were washed with PBS and stained with propidium iodide (20 μg/μL) and RNase (50 μg/μL) from Thermo Fisher Scientific for 20 min. Analysis of the labelled cells was conducted using a Guava EasyCyte 8 cell sorter (Merck Millipore, USA) and FlowJo v10 software (BD Life Sciences, USA).

3.25. Immunofluorescence

Immunofluorescence was performed using a standard protocol throughout this manuscript unless otherwise stated. The cell lines, including HCT116, A549, and MCF-7, used in this study were seeded on tissue culture plates with sterile coverslips. Plates with the cells were incubated overnight to allow adherence. The following day, cells were treated with compounds at either their IC_{50} concentration or 90 % inhibitory concentration (IC_{90}) for the period stated. Following treatment, the cells were washed in PBS and fixed with 4 % paraformaldehyde in PBS for 15 min at room temperature; permeabilization was then carried out with 0.25 % Triton X-100 in PBS for 15 min. For nonspecific antibody binding reduction, cells were pre-incubated with 3 % bovine serum albumin (BSA) in PBS for 1 h at room temperature and then incubated with the primary antibody at 37 °C in a humid chamber for 1.5 h. Following primary antibody incubation, the cells were washed and then incubated with appropriate secondary antibody overnight at 4 °C. After this, the cells were washed 3 times using PBS with Tween-20 (PBS-T) for 10 min per wash. The nuclear staining was achieved through the use of 4′,6-diamidino-2-phenylindole (DAPI) at a concentration of 0.25 μg/mL. Following incubation, the cells were mounted on slides with the same mounting medium contained, from 90 % glycerol in PBS with 2.5 % (w/v) 4-diazobicyclo-(2,2,2-octane) (DABCO). Prepared slides were further washed in PBS-T and stained with DAPI. Confocal microscopy of the immunostained sections was performed using an LSM 800 inverted laser scanning confocal microscope (Carl Zejson scanning Zeiss, Dresden, Germany) with an Airyscan detector using a 63 × 1.4 NA Plan Apochromat objective to allow for further in-depth imaging analysis. The microscopy analysis was performed using equipment funded by the Foster Foundation (USA).

3.26. Transmission electron microscopy (TEM)

After treating the cells with the specific compound, they were subjected to a series of preparatory steps essential for transmission electron microscopy. Initially, cells were rinsed with PBS, detached using trypsin, and subsequently gathered through centrifugation. For fixation, cells were immersed in 2.5 % glutaraldehyde solution (Agar Scientific), which preserves cellular structure, followed by post-fixation in a mixture of 2 % osmium tetroxide and 0.1 % potassium ferricyanide (both from Agar), enhancing electron contrast in cellular components. Next, the cells underwent a gradual dehydration process using a series of ethanol concentrations ranging from 30 % to 100 %. This step is critical to replace water in the tissue, preparing it for infiltration with resin. The dehydrated cells were then embedded in EPON resin (Agar), a procedure that provides a stable matrix for thin sectioning. The embedded samples were sectioned at a thickness of 65 nm using a Leica UC7 ultramicrotome. Sections were stained with Uranyless and Reynold's lead citrate (Delta Microscopies), which are commonly used to increase electron density in specific areas, thus improving image contrast under the electron beam. Imaging was carried out on a Tecnai Spirit BioTWIN transmission electron microscope operating at 120 kV.

3.27. Mitochondrial membrane potential

To investigate the effects of test compound (**19ba**) and (**19ca**) on mitochondrial transmembrane potential (ΔΨm) in various cancer cell lines, the 5,5,6,6′-tetrachloro-1,1′,3,3′-tetraethylbenzimi-dazoylcarbocyanine iodide (JC-1) fluorescent probe to assess cellular health and mitochondrial integrity. This probe is a critical tool for understanding mitochondrial dynamics, particularly under stress conditions induced by DNA double-strand breaks (DSBs) and its associated regulatory pathway effects. DSBs and its associated regulatory pathways are known to impact mitochondrial function negatively and can trigger mitochondrial-mediated apoptosis via the loss of ΔΨm. JC-1 dye differentially accumulates in mitochondria depending on the membrane potential; in healthy cells, it forms aggregates that emit red fluorescence, while in apoptotic or necrotic cells, the dye exists in a monomeric form in the cytosol, emitting green fluorescence. This shift from red to green fluorescence is a hallmark of mitochondrial depolarization and is quantitatively measured as a decrease in the JC-1 aggregate/monomer ratio via flow cytometry. Cells were pretreated with 10 μM Carbonyl cyanide-*p*-trifluoromethoxyphenylhydrazone (FCCP) from Sigma-Aldrich 30 min before concluding the incubation with the target drug. FCCP also served as a positive control at the same concentration. Following this treatment, the culture medium was exchanged for fresh medium containing 5 μg/ml JC-1 dye, also sourced from Sigma-Aldrich. Cells were then incubated in darkness at 37 °C for 20 min. After incubation, cells underwent two washes with PBS before their fluorescence was quantitatively measured.

3.28. Apoptosis evaluation

To evaluate the proapoptotic effects of specific compounds, cellular assays were executed using established protocols. Cells were initially plated on appropriate Petri dishes and allowed to adhere overnight. These cells were then exposed to the compounds at their respective IC_{50} concentrations for durations of 24 and 48 h. For control purposes, 1 % DMSO (Merck) and 1 μM MTX (Sigma-Aldrich) served as reference substances. Post-treatment, cells were collected and stained with FITC-Annexin V (Thermo Fisher, V13242) according to the manufacturer's guidelines. To distinguish viable from non-viable cells, subsequent staining with propidium iodide (Thermo Fisher) was conducted. Analysis of the stained cells was performed using a Guava easyCyte 8 flow cytometer (Merck Millipore). Data from these experiments were then processed and analyzed using FlowJo v10 software, which facilitated a detailed assessment of apoptotic activity relative to the controls.

3.29. Ex-ovo CAM assay

Fertilized chicken eggs were sourced from a local supplier and incubated at 37.5 °C with a humidity of 65 % and periodic rotation for three days. On the third day, the eggs were carefully opened into sterile weighing boats, each covered with a sterile lid, and placed in a cell culture-grade CO_2 incubator maintained at 37 °C and 5 % CO_2 concentration. To assess the angiogenic potential of various compounds, on the seventh day, glass filter paper discs, previously dipped in designated drug concentrations and dried, were applied to the chorioallantoic membrane (CAM) vascular zones. The development of the vascular networks was monitored, and images were captured periodically. These images were subsequently analyzed using AngioTool software to quantify vascular growth. On the eighth day of incubation, additional CAM models were used for tumor cell inoculation. Each model received a mixture of 2,000,000 tumor cells and Matrigel (Corning), precisely deposited on the CAM. After a 48-h incubation period, a sterile silicone ring was positioned at the inoculation site, and the prepared drug solution, diluted in sterile normal saline, was administered within the ring. Post-treatment, the embryos were sacrificed by cutting the vitelline arteries. The tumors were then excised, weighed, and fixed in 4 % paraformaldehyde (PFA). Subsequently, they were sectioned using a Leica cryotome. Standard hematoxylin and eosin (H&E) staining was performed on the tissue sections for histological analysis. The CAM experiments are not considered to be animal experimentation from a regulatory point of view in Europe (EU directive 2010/63/EU), European Commission (2021/2784(RSP)). This method offers several advantages that extend beyond its simplicity and cost-effectiveness. Notably, it facilitates rapid xenografting of tumor cells and the development of tumors, allows for the observation of metastatic processes and angiogenesis, and supports the thorough assessment of drug characterization and delivery mechanisms [33,34].

4. Conclusion

The studies presented in this manuscript provide a profound insight into the cytotoxic and mechanistic effects of two novel compounds, (**19ba**) and (**19ca**), on various cancer cell lines, including MCF-7 (breast adenocarcinoma), A549 (non-small cell lung carcinoma), and HCT116 (colon carcinoma). These compounds were evaluated for their ability to induce cytotoxicity, impact cellular morphology, inhibit colony formation, affect cell cycle progression, induce DNA damage, alter mitochondrial dynamics, and trigger apoptosis. The cytotoxicity assessments demonstrated that both (**19ba**) and (**19ca**) selectively inhibit cell viability in a dose-dependent manner across different cell lines with notable specificity and potency. Particularly, (**19ca**) showed remarkably low IC_{50} values on MCF-7 and A549 cells compared to (**19ba**), indicating a stronger cytotoxic effect on these cell types. The morphological evaluations using phase contrast and fluorescence microscopy revealed significant changes indicative of apoptosis, such as cell shrinkage, nuclear condensation, and membrane blebbing, further confirming the cytotoxic nature of these compounds. In terms of colony formation, both compounds significantly reduced the clonogenic potential of the treated cell lines, with (**19ca**) exhibiting a more pronounced effect on MCF-7 and A549 cells. This suggests that these compounds not only kill cancer cells but also prevent their proliferation, a key factor in cancer progression and metastasis. Analysis of cell cycle progression indicated that (**19ba**) and (**19ca**) disrupt the normal cell cycle, causing accumulation of cells in specific phases, which correlates with the induction of cytotoxic stress. The flow cytometric analysis of DNA damage highlighted an increased presence of γH2AX foci, a marker for DNA breaks, particularly in cells treated with (**19ca**), suggesting a robust mechanism of action involving DNA damage pathways. Furthermore, the studies on mitochondrial dynamics revealed that both compounds cause significant changes in mitochondrial membrane potential, indicative of mitochondrial dysfunction and apoptosis. This was complemented by the observation of cytochrome *c* release from mitochondria, a key step in the apoptosis pathway (Fig. 10). The *ex ovo* assessments using the chorioallantoic membrane (CAM) assay demonstrated that (**19ca**) reduces angiogenesis and tumor growth, which is crucial for its potential application in anti-cancer therapy. In contrast, (**19ba**) showed significant embryotoxicity, limiting its *ex ovo* applicability but underscoring the importance of dosage and delivery method optimization.

While the exact molecular targets of these compounds were not defined in this study, literature suggests that carbazole derivatives may exhibit specificity towards various molecular targets. These targets include tubulin, topoisomerases, histone deacetylases (HDACs), receptor tyrosine kinases (RTKs), heat shock proteins (HSPs), cyclin-dependent kinases (CDKs) and others [35]. Each of these targets plays a critical role in cellular processes such as cell division, DNA replication, gene expression, signal transduction, and protein folding. Given the observed effects of (**19ba**) and (**19ca**) on cell viability, DNA damage, and mitochondrial dysfunction, it is plausible that these compounds interact with one or more of these targets. However, due to the complexity and multiplicity of these pathways, it is challenging to conclusively confirm any specific target based on the current results. The observed cytotoxic and mechanistic effects suggest potential multi-target interactions, but further studies involving target-specific assays and molecular docking studies are necessary to elucidate the exact mechanisms of action.

These findings highlight the potential of compounds (**19ba**) and (**19ca**) as promising therapeutic agents. They exhibit a multifaceted mechanism of action, including direct cytotoxic effects, inhibition of colony formation, disruption of the cell cycle, induction of DNA damage, and triggering of apoptosis pathways. These mechanisms collectively contribute to their potent anti-cancer properties. The results presented here not only enhance our understanding of the therapeutic potential of these compounds but also provide a basis for further preclinical and clinical evaluations. It is crucial that subsequent studies focus on optimizing the pharmacokinetic properties of these compounds, exploring their efficacy in combination drug treatments, and conducting

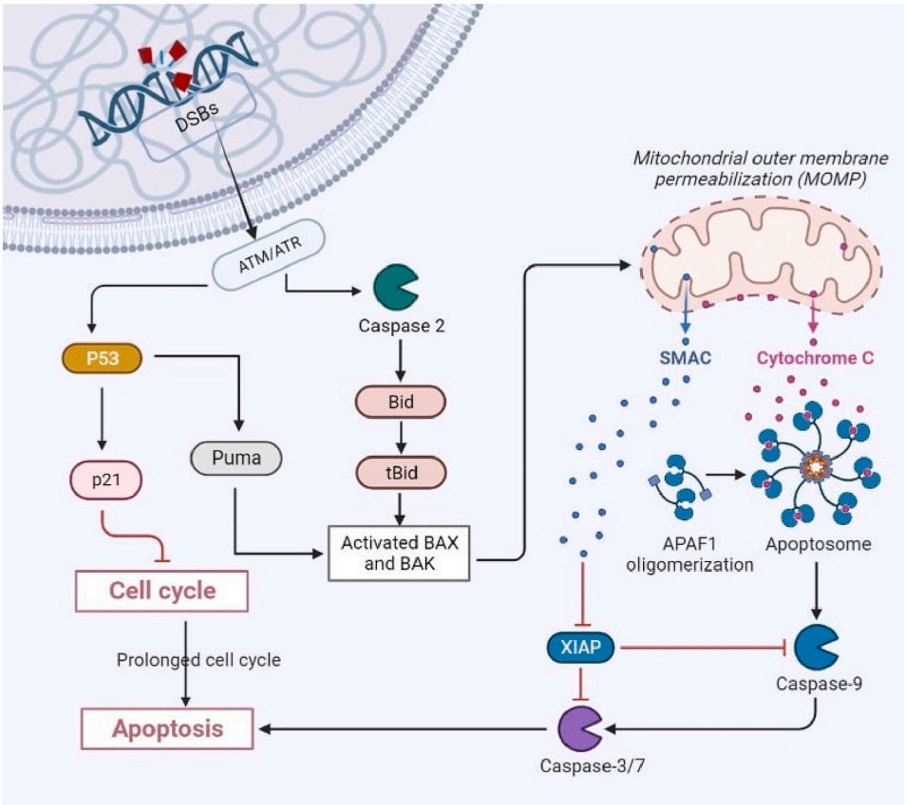

Fig. 10. Possible mechanism of DNA damage and mitochondrial disruption caused by (**19 ab**) and (**19ac**) molecules.

comprehensive *in vivo* studies to evaluate their safety and effectiveness in clinical settings. This integrative approach will be crucial in transitioning these compounds from the bench to bedside, offering new avenues for cancer treatment that may overcome the limitations of current therapies. Additionally, in the context of chemical synthesis, it is necessary to obtain more thioamide derivatives of tetrahydrocarbazole. Finding convenient thionation methods and attempting to obtain more structurally complex chemical molecules will help in determining how to modify the tetrahydrocarbazole skeleton to enhance its anticancer activity.

CRediT authorship contribution statement

Alicja Trocka: Writing – original draft, Methodology, Investigation. **Anoop Kallingal:** Writing – original draft, Methodology, Investigation, Conceptualization. **Natalia Maciejewska:** Investigation, Data curation. **Magdalena Narajczyk:** Visualization, Investigation. **Anna Hromova:** Investigation. **Sławomir Makowiec:** Writing – original draft, Supervision, Methodology, Investigation, Data curation, Conceptualization.

Declaration of competing interest

The authors declare that they have no known competing financial interests or personal relationships that could have appeared to influence the work reported in this paper.

Data availability

Data will be made available on request.

Acknowledgements

The financial support to maintenance of research facilities used in these studies from Gdańsk University of Technology by the DEC-2/2021/IDUB/V.6/Si grant under the SILICIUM SUPPORTING CORE R&D FACILITIES “Excellence Initiative—Research University” program is gratefully acknowledged.

Appendix A. Supplementary data

Supplementary data to this article can be found online at https://doi.org/10.1016/j.ejmech.2024.116755.

References

[1] T.Y. Chaudhari, V. Tandon, Recent approaches to the synthesis of tetrahydrocarbazoles, Org, Biomol. Chem. 19 (2021) 1926–1939, https://doi.org/10.1039/D0OB02274H.
[2] H.-J. Knölker, K.R. Reddy, Chapter 4 - biological and pharmacological activities of carbazole alkaloids, in: G.A. Cordell (Ed.), The Alkaloids: Chemistry and Biology, Academic Press, 2008, pp. 181–193, https://doi.org/10.1016/S1099-4831(07)00004-1.
[3] Sibaji Sarkar, Shubham Makvana, Disha Hirani, Isha Makadia, Khyati Dholariya, Harsh Dhokia, Nency Vanpariya, Tetrahydrocarbazoles as potential therapeutic agents: a review of their synthesis and biological activities, World J. Adv. Res. Rev. 21 (2023) 2127–2135, https://doi.org/10.30574/wjarr.2024.21.3.0935.
[4] G. Allais, C. Benedetto, Spotlight on frovatriptan: a review of its efficacy in the treatment of migraine, Drug Des. Dev. Ther. 10 (2016) 3225–3236, https://doi.org/10.2147/DDDT.S105932.
[5] M.I. Wilde, A. Markham, Ondansetron. A review of its pharmacology and preliminary clinical findings in novel applications, Drugs 52 (1996) 773–794, https://doi.org/10.2165/00003495-199652050-00010.
[6] A. Caruso, J. Ceramella, D. Iacopetta, C. Saturnino, M.V. Mauro, R. Bruno, S. Aquaro, M.S. Sinicropi, Carbazole derivatives as antiviral agents: an overview, Molecules 24 (2019) 1912, https://doi.org/10.3390/molecules24101912.
[7] Z. Yin, L.R. Whittell, Y. Wang, S. Jergic, M. Liu, E.J. Harry, N.E. Dixon, J.L. Beck, M.J. Kelso, A.J. Oakley, Discovery of lead compounds targeting the bacterial sliding clamp using a fragment-based approach, J. Med. Chem. 57 (2014) 2799–2806, https://doi.org/10.1021/jm500122r.
[8] L. Su, J. Li, Z. Zhou, D. Huang, Y. Zhang, H. Pei, W. Guo, H. Wu, X. Wang, M. Liu, C.-G. Yang, Y. Chen, Design, synthesis and evaluation of hybrid of tetrahydrocarbazole with 2,4-diaminopyrimidine scaffold as antibacterial agents, Eur. J. Med. Chem. 162 (2019) 203–211, https://doi.org/10.1016/j.ejmech.2018.11.016.
[9] N. Mohamed, W. El-Serwy, S. Abd El-Karim, G. Awad, S. Elseginy, Synthesis, antimicrobial evaluation, and molecular docking studies of new tetrahydrocarbazole derivatives, Res. Chem. Intermed. 42 (2015), https://doi.org/10.1007/s11164-015-2090-6.
[10] S.K. Lee, J. Xing, I.M. Catlett, R. Adamczyk, A. Griffies, A. Liu, B. Murthy, M. Nowak, Safety, pharmacokinetics, and pharmacodynamics of BMS-986142, a novel reversible BTK inhibitor, in healthy participants, Eur. J. Clin. Pharmacol. 73 (2017) 689–698, https://doi.org/10.1007/s00228-017-2226-2.
[11] Z. Fan, V. Calsolaro, R.A. Atkinson, G.D. Femminella, A. Waldman, C. Buckley, W. Trigg, D.J. Brooks, R. Hinz, P. Edison, Flutriciclamide (^{18}F-GE180) PET: first-in-human PET study of novel third-generation in vivo marker of human translocator protein, J. Nucl. Med. 57 (2016) 1753–1759, https://doi.org/10.2967/jnumed.115.169078.
[12] S. Karwehl, R. Jansen, V. Huch, M. Stadler, Sorazolons, carbazole alkaloids from sorangium cellulosum strain Soce375, J. Nat. Prod. 79 (2016), https://doi.org/10.1021/acs.jnatprod.5b00997.
[13] J. Chen, J.-J. Chen, X. Yao, K. Gao, Kopsihainanines A and B, two unusual alkaloids from Kopsia hainanensis, Org. Biomol. Chem. 9 (2011) 5334–5336, https://doi.org/10.1039/C1OB05724C.
[14] M. Motegi, A. Nugroho, Y. Hirasawa, T. Arai, A.H. Hadi, H. Morita, Leucomidines A–C, novel alkaloids from Leuconotis griffithii, Tetrahedron Lett. 53 (2012) 1227–1230, https://doi.org/10.1016/j.tetlet.2011.12.116.
[15] H. Pei, J. Qin, F. Wang, B. Tan, Z. Zhao, Y. Peng, F. Yu, E. Li, M. Liu, R. Zhang, B. Liu, B. Du, Y. Chen, Discovery of potent ureido tetrahydrocarbazole derivatives for cancer treatments through targeting tumor-associated macrophages, Eur. J. Med. Chem. 183 (2019) 111741, https://doi.org/10.1016/j.ejmech.2019.111741.
[16] H.B. El-Nassan, Synthesis and antitumor activity of tetrahydrocarbazole hybridized with dithioate derivatives, J. Enzym. Inhib. Med. Chem. 30 (2015) 308–315, https://doi.org/10.3109/14756366.2014.922554.
[17] J.R. Woods, M.V. Riofski, M.M. Zheng, M.A. O’Banion, H. Mo, J. Kirshner, D. A. Colby, Synthesis of 15-methylene-eburnamonine from (+)-vincamine, evaluation of anticancer activity, and investigation of mechanism of action by quantitative NMR, Bioorg. Med. Chem. Lett 23 (2013), https://doi.org/10.1016/j.bmcl.2013.08.095.
[18] J. Chen, J. Lou, T. Liu, R. Wu, X. Dong, Q. He, B. Yang, Y. Hu, Synthesis and in-vitro antitumor activities of some mannich bases of 9-alkyl-1,2,3,4-tetrahydrocarbazole-1-ones, Arch. Pharm. (Weinheim) 342 (2009) 165–172, https://doi.org/10.1002/ardp.200800179.
[19] M. Witkowska, N. Maciejewska, M. Ryczkowska, M. Olszewski, M. Bagiński, S. Makowiec, From tryptophan to novel mitochondria-disruptive agent, synthesis and biological evaluation of 1,2,3,6-tetrasubstituted carbazoles, Eur. J. Med. Chem. 238 (2022) 114453, https://doi.org/10.1016/j.ejmech.2022.114453.
[20] J.J. Li, Borsche–drechsel cyclization, in: J.J. Li (Ed.), Name Reactions: A Collection of Detailed Mechanisms and Synthetic Applications, fifth ed., Springer International Publishing, Cham, 2014, pp. 68–69, https://doi.org/10.1007/978-3-319-03979-4_33.
[21] H.K. Grover, T.P. Lebold, M.A. Kerr, Tandem cyclopropane ring-opening/conia-ene reactions of 2-alkynyl indoles: a [3 + 3] annulative route to tetrahydrocarbazoles, Org. Lett. 13 (2011) 220–223, https://doi.org/10.1021/ol102627e.
[22] P. Tharra, B. Baire, Regioselective cyclization of (Indol-3-yl)pentyn-3-ols as an approach to (Tetrahydro)carbazoles, Org. Lett. 20 (2018) 1118–1121, https://doi.org/10.1021/acs.orglett.8b00042.
[23] F. Zhan, G. Liang, Formation of enehydrazine intermediates through coupling of phenylhydrazines with vinyl halides: entry into the fischer indole synthesis, Angew. Chem. 125 (2013) 1304–1307, https://doi.org/10.1002/ange.201207173.
[24] L.N. Nanda, V.A. Rangari, TfOH catalyzed synthesis of 1-substituted tetrahydrocarbazoles, Tetrahedron Lett. 59 (2018) 3194–3197, https://doi.org/10.1016/j.tetlet.2018.07.023.
[25] H. Mei, Y. Yu, C. Wang, A. Liu, J. Han, Assembly of tetracyclic tetrahydrocarbazoles via a visible-light promoted cascade process, Org. Chem. Front. 9 (2022) 2516–2521, https://doi.org/10.1039/D2QO00247G.
[26] Y. Qiu, K.T. Puni, C.C. Duplan, A.C. Lindsay, J. Sperry, Tetrahydrocarbazoles by mechanochemical Fischer indolisation, Tetrahedron Lett. 72 (2021) 153068, https://doi.org/10.1016/j.tetlet.2021.153068.
[27] J. He, A. Liu, Y. Yu, C. Wang, H. Mei, J. Han, Electrochemical annulation of indole-tethered alkynes enabling synthesis of exocyclic alkenyl tetrahydrocarbazoles, J. Org. Chem. 88 (2023) 6962–6972, https://doi.org/10.1021/acs.joc.3c00267.
[28] B. Robinson, The fischer indole synthesis, Chem. Rev. 63 (1963) 373–401, https://doi.org/10.1021/cr60224a003.
[29] N. Mahanta, D.M. Szantai-Kis, E.J. Petersson, D.A. Mitchell, Biosynthesis and chemical applications of thioamides, ACS Chem. Biol. 14 (2019) 142–163, https://doi.org/10.1021/acschembio.8b01022.
[30] K.M. Tveit, E.O. Pettersen, S.D. Fosså, A. Pihl, Selection of tumour cell subpopulations occurs during cultivation of human tumours in soft agar. A DNA flow cytometric study, Br. J. Cancer 52 (1985) 701–705, https://doi.org/10.1038/bjc.1985.246.
[31] V. Hug, M. Haynes, R. Rashid, G. Spitzer, G. Blumenschen, G. Hortobagyi, Improved culture conditions for clonogenic growth of primary human breast tumours, Br. J. Cancer 50 (1984) 207–213, https://doi.org/10.1038/bjc.1984.164.
[32] T. Eleftheriadis, G. Pissas, V. Liakopoulos, I. Stefanidis, Cytochrome c as a potentially clinical useful marker of mitochondrial and cellular damage, Front. Immunol. 7 (2016), https://doi.org/10.3389/fimmu.2016.00279.
[33] D. Fischer, G. Fluegen, P. Garcia, N. Ghaffari-Tabrizi-Wizsy, L. Gribaldo, R.Y.-J. Huang, V. Rasche, D. Ribatti, X. Rousset, M.T. Pinto, J. Viallet, Y. Wang,

R. Schneider-Stock, The CAM model—Q&A with experts, Cancers 15 (2022) 191, https://doi.org/10.3390/cancers15010191.

[34] K. Mitrevska, M.A. Merlos Rodrigo, N. Cernei, H. Michalkova, Z. Splichal, D. Hynek, O. Zitka, Z. Heger, P. Kopel, V. Adam, V. Milosavljevic, Chick chorioallantoic membrane (CAM) assay for the evaluation of the antitumor and antimetastatic activity of platinum-based drugs in association with the impact on the amino acid metabolism, Mater Today Bio 19 (2023) 100570, https://doi.org/10.1016/j.mtbio.2023.100570.

[35] S. Issa, A. Prandina, N. Bedel, P. Rongved, S. Yous, M. Le Borgne, Z. Bouaziz, Carbazole scaffolds in cancer therapy: a review from 2012 to 2018, J. Enzyme Inhib. Med. Chem. 34 (2019) 1321–1346, https://doi.org/10.1080/14756366.2019.1640692.